Received: 5 July 2019 | Revised: 25 July 2019 | Accepted: 25 July 2019

DOI: 10.1002/cne.24756

RESEARCH ARTICLE

JCN RESEARCH IN SYSTEMS NEUROSCIENCE THE JOURNAL OF COMPARATIVE NEUROLOGY WILEY

# Characterizing the morphology of somatostatin-expressing interneurons and their synaptic innervation pattern in the barrel cortex of the GFP-expressing inhibitory neurons mouse

Xiaojuan Zhou | Ima Mansori | Tatjana Fischer | Mirko Witte | Jochen F. Staiger

Institute for Neuroanatomy, University Medical Center Göttingen, Georg-August-University, Göttingen, Germany

**Correspondence**
Jochen Staiger, Institute for Neuroanatomy, University Medical Center Göttingen, Georg-August-University, Kreuzberging 36, D-37075 Göttingen, Germany.
Email: jochen.staiger@med.uni-goettingen.de

**Funding information**
Deutsche Forschungsgemeinschaft, Grant/Award Numbers: CRC 889, STA 431/14-1

## Abstract

Somatostatin-expressing (SST+) cells form the second largest subpopulation of neocortical GABAergic neurons that contain diverse subtypes, which participate in layer-specific cortical circuits. Martinotti cells, as the most abundant subtype of SST+ interneurons, are mainly located in layers II/III and V/VI, and are characterized by dense axonal arborizations in layer I. GFP-expressing inhibitory neurons (GIN), representing a fraction of mainly upper layer SST+ interneurons in various cortical areas, were recently claimed to include both Martinotti cells and non-Martinotti cells. This makes it necessary to examine in detail the morphology and synaptic innervation pattern of the GIN cells, in order to better predict their functional implications. In our study, we characterized the neurochemical specificity, somatodendritic morphology, synaptic ultrastructure as well as synaptic innervation pattern of GIN cells in the barrel cortex in a layer-specific manner. We showed that GIN cells account for 44% of the SST+ interneurons in layer II/III and around 35% in layers IV and Va. There are 29% of GIN cells coexpressing calretinin with 54% in layer II/III, 8% in layer IV, and 13% in layer V. They have diverse somatodendritic configurations and form relatively small synapses across all examined layers. They almost exclusively innervate dendrites of excitatory cells, preferentially targeting distal apical dendrites and apical dendritic tufts of pyramidal neurons in layer I, and rarely target other inhibitory neurons. In summary, our study reveals unique features in terms of the morphology and output of GIN cells, which can help to better understand their diversity and structure–function relationships.

**KEYWORDS**

barrel cortex, electron microscopy, GABA immunogold labeling, GIN transgenic mice, RRID: AB_10000321, RRID: AB_221569, RRID: AB_304897, RRID: AB_477652, somatostatin-positive neurons, synapse

## 1 | INTRODUCTION

Martinotti cells were first discovered in the late 19th century by Carlo Martinotti and are characterized by extensive axonal ramifications in layer I (Fairen, DeFelipe, & Regidor, 1984). Nowadays, it is known that Martinotti cells form the majority of somatostatin-expressing (SST+) interneurons, which are one of the three nonoverlapping classes of cortical interneurons, in addition to parvalbumin-expressing (PV+)

interneurons and vasoactive intestinal polypeptide-expressing (VIP+) interneurons (Rudy, Fishell, Lee, & Hjerling-Leffler, 2011; Tasic et al., 2018; Tremblay, Lee, & Rudy, 2016). Like the other classes, SST+ interneurons are diverse in molecular, morphological, and electrophysiological features (Ascoli et al., 2008; DeFelipe et al., 2013; Urban-Ciecko & Barth, 2016). They can co-express other molecular markers, such as calretintin (CR), calbindin (CB), neuropeptide Y (NPY), and neuronal nitric oxide synthase (nNOS), and show a layer-specific distribution of their subtypes in various cortical regions (Gonchar, Wang, & Burkhalter, 2008; He et al., 2016; Xu, Roby, & Callaway, 2006).

There are SST-Cre transgenic mice, which label the whole population of SST+ interneurons and three transgenic mouse lines, namely GIN, X94, and X98, which label more or less nonoverlapping subpopulations of SST+ interneurons in different cortical layers (Ma, Hu, Berrebi, Mathers, & Agmon, 2006; Oliva, Jiang, Lam, Smith, & Swann, 2000; Taniguchi et al., 2011). The GFP-expressing neurons in the GIN mouse preferentially label Martinotti cells in layers II/III and Va. In contrast, the GFP-expressing cells in the X98 and X94 mouse lines mainly represent Martinotti cells in deep layers and quasi-fast spiking non-Martinotti cells in layer IV, respectively (Emmenegger, Qi, Wang, & Feldmeyer, 2018; Nigro, Hashikawa-Yamasaki, & Rudy, 2018). These subpopulations of SST+ neurons integrate into different cortical circuits and display a layer-specific modulation of their activity in the behaving animals (Muñoz, Tremblay, Levenstein, & Rudy, 2017; Silberberg & Markram, 2007; Xu, Jeong, Tremblay, & Rudy, 2013).

Martinotti cells are considered as dendrite-targeting interneurons (Markram et al., 2004). They mainly innervate dendrites of pyramidal neurons as shown by a few ultrastructural studies in the hippocampus and various cortical regions (de Lima & Morrison, 1989; Katona, Acsády, & Freund, 1999; Melchitzky & Lewis, 2008; Wang et al., 2004). In the mouse barrel cortex, layer II/III SST+ interneurons, most (if not all) representing Martinotti cells, are spontaneously active in the quiet-awake state, however, during active whisking, these neurons get suppressed in activity (Gentet et al., 2012; Muñoz et al., 2017). Thus, this should release dendritic inhibition of pyramidal neurons and facilitate sensory processing. Inhibition of SST+ cells has been shown to be mediated by VIP+ and PV+ interneurons via different disinhibitory circuit motifs (Karnani et al., 2016; Lee, Kruglikov, Huang, Fishell, & Rudy, 2013; Pi et al., 2013; Walker et al., 2016).

However, studies of interneuron connectivity found that layer II/III SST+ interneurons also inhibit different types of interneurons in the mouse visual cortex and barrel cortex (Jiang et al., 2015; Jiang, Wang, Lee, Stornetta, & Zhu, 2013; Karnani et al., 2016; Pfeffer, Xue, He, Huang, & Scanziani, 2013). Unlike layer II/III SST+ interneurons, layer IV SST+ cells form a disinhibitory motif by primarily inhibiting the PV+ interneurons (Xu et al., 2013), which is in agreement with a recent study showing that layer IV SST+ interneurons in the mouse somatosensory cortex (S1) are all non-Martinotti cells (Scala et al., 2018). Instead of being entirely homogeneous, several studies using GIN mice found morphologically and electrophysiologically diverse subtypes of layer II/III SST+ interneurons (Halabisky, Shen, Huguenard, & Prince, 2006; McGarry et al., 2010; Riedemann, Straub, & Sutor, 2018; Xu et al., 2006). Additionally, GIN cells coexpressing CR were reported to differ from CR-immunonegative GIN cells by having more primary dendrites and more horizontal dendritic fields (Xu et al., 2006). Another level of inhomogeneity of GIN cells is suggested by the area-specific presence of non-Martinotti cells in layer IV of barrel cortex (Emmenegger et al., 2018; Scala et al., 2018).

Here, we characterized the neurochemical profile, morphology, and synaptic innervation of GIN cells of all layers of the mouse barrel cortex. We found that GIN cells accounted for 21% of SST+ interneurons in total by forming 44% of the SST+ interneurons in layer II/III and around 35% in layers IV and Va. CR-expressing GIN cells constituted 29% of all GIN cells, with 54% in layer II/III, 8% in layer IV, and 13% in layer V. GIN cells are preferentially multipolar neurons but also show different other types of somatodendritic configurations throughout all examined layers. They possess relatively small presynaptic boutons, which form synapses with short postsynaptic densities on their subcellular target structures, when compared to VIP+ neurons. GIN cells innervate mainly dendritic shafts and to a lesser extent dendritic spines but not somata. Most of the targeted dendrites are GABA-immunonegative, which are likely to belong to the distal apical dendrites of pyramidal neurons. Our study reveals unique features in terms of morphology and output of GIN cells in the mouse barrel cortex, which can help better understand their diversity and structure–function relationships.

## 2 | MATERIALS AND METHODS

### 2.1 | Animals, perfusion, and tissue processing

Homozygous GIN mice (FVB-Tg(GadGFP)45704Swn) were used in this study. All mice were bred at the animal facility of the University Medical Center Göttingen (Germany). The experimental procedures were performed in accordance with German laws on animal research (TierSchG und TierSchVersV 2013). All mice were anesthetized by an overdose of ketamine and transcardially perfused. For fluorescence immunohistochemistry, 11 GIN mice were perfused with 10% sucrose for 1 min, followed by 4% paraformaldehyde (PFA) in phosphate buffer (PB, pH 7.4) for 20 min. After perfusion, the brains were dissected and postfixed in perfusion solution for 2 hr at 4°C. For ultrastructural studies, six GIN mice were perfused with 0.9% sodium chloride for 1 min, and acidic fixative (2% PFA, 1% glutaraldehyde [GA], in sodium acetate buffer, pH 6.0) for 1 min and basic fixative (2% PFA, 1% GA, in borate buffer, pH 8.5) for 1 hr. After fixation, the brains were washed in PB and sectioned into 50 μm-thick coronal sections with a vibratome (VT 1200S; Leica, Germany). The sections from Bregma −1.22 mm to Bregma −1.94 mm were used for immunohistochemical staining.

### 2.2 | Immunohistochemistry

#### 2.2.1 | Double immunofluorescence staining

To study the distribution and colocalization of GIN cells with somatostatin and calretinin, we performed double immunofluorescence staining on GIN mouse sections. They were washed in 0.05 M tris

buffer (TB), 0.05 M tris-buffered saline (TBS), and tris-buffered saline containing 0.5% triton (TBST) and incubated in a blocking solution (TBST with 10% normal donkey serum and 0.25% bovine serum albumine) for 90 min at room temperature. The primary antibodies were goat anti-GFP (1:2,000; Abcam, UK), rabbit anti-SST 14 (1:5,000; Bachem, Switzerland), and anti-CR (1:2,000; Swant, Switzerland). After incubation for 36–72 hrs at 4°C, they were washed in TBS. The secondary antibodies were donkey anti-goat (1:500; Alexa Fluor 488, Life Technologies, Darmstadt, Germany) and donkey anti-rabbit (1:500; Alexa Fluor 594, Life Technologies). After incubation for 4 hrs at room temperature in the dark, they were washed in TBS and stained with 4′,6-Diamidin-2-phenylindol (DAPI) (1:1,000 in TBS) for 5 min. The sections were then rinsed in TBS and TB and mounted on slides with Aqua Poly-Mount (Polyscience).

### 2.2.2 | Immunostaining with DAB-peroxidase

To study the ultrastructure of GIN cells, we performed anti-GFP immunohistochemistry with DAB-peroxidase. Before staining, the sections were first incubated in a cryoprotectant (25% saccharose and 10% glycerol in 0.01 M PB) overnight at 4°C and freeze-thawed three times over liquid nitrogen. Then they were incubated in a blocking solution for 4 hrs at room temperature (0.25% bovine serum albumin, 0.1 M DL-lysin, and 10% normal goat serum in 0.05 M TBS pH 7.6) and stained with primary antibody (rabbit anti-GFP, Invitrogen, A11122, 1:1,000 diluted) for 72 hrs at 4°C. Afterward, they were stained with the secondary antibody (biotinylated goat anti-rabbit, 1:200 diluted) overnight at 4°C, followed by an incubation with avidin-biotin complex (ABC) solution (Vector Laboratories, CA, 1:400 diluted) overnight at 4°C. Finally, they were incubated in 1 mg/mL 3–3′ diaminobenzidine tetrahydrochloride (DAB; Sigma, Germany) for 10 min. The reaction was started by adding $H_2O_2$ to a concentration of 0.01%, lasted for 7–10 min, and was stopped by rinsing in TB.

### 2.2.3 | Post-embedding anti-GABA immunogold staining

Post-embedding anti-GABA immunogold staining was modified from the study by Somogyi, Hodgson, Chubb, Penke, and Erdei (1985) and described in detail in our previous study (Zhou, Rickmann, Hafner, & Staiger, 2017). Electron microscopic sample preparation procedure was performed as follows. The grids were etched by periodic acid and sodium periodate to get rid of the osmium and the resin. After rinsing in distilled water and TBS (pH 7.4), they were blocked with 1% ovalbumine in TBS for 30 min and incubated in the primary antibody (polyclonal rabbit anti-GABA, Sigma-Aldrich, A2052; 1:500 to 1:1,000 diluted) for 90 min at room temperature or overnight at 4°C. After rinsing, they were labeled with the secondary antibody (goat anti-rabbit conjugated with 12 nm gold, Dianova No. 111-205-144, 1:20 dilution) for 90 min in a dark moist chamber. After rinsing, the grids were contrast stained with 10% uranyl acetate for 30 min and rinsed four times in distilled water.

### 2.2.4 | Staining of biocytin-filled pyramidal neuron

A GIN mouse was deeply anesthetized with isoflurane and decapitated. Coronal slices (of 300 μm thickness) containing the barrel cortex were cut using a vibratome (VT 1200S; Leica). Slices were transferred to a chamber for whole-cell patch-clamp recording. Afterward, the slices were placed in fixative (2% PFA and 1% GA in PB) overnight at 4°C. Pyramidal neurons in layer II/III were recorded for 15–20 min and filled with biocytin. The biocytin staining has been described previously in detail (Staiger et al., 2004). In brief, after washing in PB, slices were treated with 1% $H_2O_2$ to block endogenous peroxidase activity. They were incubated in the cryoprotectant and freeze-thawed three times over liquid nitrogen. After rinsing, they were incubated in the ABC solution and the DAB-peroxidase reaction was carried out by the same procedure as described previously. After biocytin staining, the pyramidal cells were imaged for performing correlated light and electron microscopy. Then, anti-GFP DAB-peroxidase immunohistochemistry was used to stain the GIN cells and their processes in the slices, as described previously.

### 2.2.5 | Antibody specificity

We used goat anti-GFP (Abcam, cat# ab5450, RRID: AB_304897) at 1:2,000 dilution and rabbit anti-GFP (Invitrogen, cat# A11122, RRID: AB_221569) at 1:1,000 dilution to detect GFP by immunohistochemistry in the perfusion-fixed brain sections. We used the same antibodies to stain GIN cells as we previously did for VIP+ interneurons in VIP-Cre/Rosa-YFP transgenic mice (Walker et al., 2016; Zhou et al., 2017). Rabbit anti-SST 14 (Bachem, cat# H-1490) was used at 1:5,000 dilution to stain somatostatin-expressing neurons. This antibody shows reliable staining of SST+ neurons in various brain regions (Domínguez, Morona, González, & Moreno, 2013; Ohira, Takeuchi, Iwanaga, & Miyakawa, 2013). To stain CR+ cells, we used the rabbit anti-CR (Swant, Cat# 7699/3H, RRID: AB_10000321) at 1:2,000 dilution. The specificity and sensitivity of this antibody were reliably shown in plenty of studies (Riedemann, Schmitz, & Sutor, 2016; Xu et al., 2006). Rabbit anti-GABA (Sigma-Aldrich; A2052, RRID: AB_477652) was used at 1:500 to 1:1,000 dilution to detect GABA+ subcellular profiles by post-embedding immunohistochemistry. The antibody specificity and sensitivity was quantitatively analyzed in our previous study (Zhou et al., 2017).

## 2.3 | Image acquisition and data analysis

Fluorescent immunopositive cells were imaged with an upright epifluorescence microscope (AxioImager.M2, Zeiss, Germany), using structured illumination (ApoTome, Zeiss) operated by Neurolucida software (MBF Bioscience, Colchester, VT). DAPI staining was used to delineate the layers of the barrel cortex. Quantification in terms of GFP+ cells, SST+ cells, and their colocalization was performed using the Neurolucida software from 24 sections of 8 GIN mice with a counting frame consisting of at least three to four barrel-related columns in each section. The colocalization ratio of GIN cells and CR+ cells was quantified from 10 sections of 3 GIN mice under the same approach.

The overview images of GIN cells were taken from a light microscope in brightfield mode (Axioskop, Zeiss) with a ×10 objective lens at various exposure times, to compensate for steep illumination gradients at the slice surface or at larger blood vessels within the tissue. The final overview image was merged by blending the images using the EnfuseGUI software. We used an inverted epi-fluorescence microscope (Axio Observer Z1, Zeiss) with a ×63 objective (water immersion, NA = 1.2) and Zen blue software (Zen 2.3, Pro, Zeiss) to obtain image stacks of biocytin-filled GIN cells and pyramidal neurons. Neurolucida reconstruction was done either using the image stacks or using the live mode on a microscope with a ×63 objective (Axioskop 2 Mot Plus, Zeiss, ×63 water immersion, NA = 1.2). The axonal bouton density was quantified in layers I–Va using three GIN mice. The counting volumes contained ~100 μm (x-dimension) × layer length (μm, y-dimension) × 10 μm (z-dimension). The density was analyzed as boutons/(10 μm)$^3$.

## 2.4 | Electron microscopic sample preparation and imaging acquisition

After immunostaining, the 50 μm-thick sections and the 300 μm-thick slices containing biocytin-filled pyramidal neurons were treated with 0.5% osmium tetroxide for 1 hr and washed intensively in phosphate-buffered saline (PBS). The sections were then dehydrated and infiltrated with resin by the following protocol: 30% 5 min, 50% 5 min, 70% 30 min, 90% 10 min, 100% 10 min, isopropanol 10 min, propylene oxide 2 × 10 min, propylene oxide/epoxy resin (1:1) 60 min, epoxy resin overnight, and fresh epoxy resin 4 hr. The sections and the slices were flat embedded in epoxy resin on slides and polymerized at 60°C for 2 days.

For the quantitative analysis of the synaptic innervation pattern by GIN presynaptic boutons, one to two sections of six GIN mice barrel cortex were re-embedded into epoxy resin-filled capsule blocks. We trimmed the blocks into 700 μm × 300 μm large trapezoid-shaped pyramids containing cortical layers I–Va of the barrel cortex. Two to three consecutive ultrathin sections were cut on an ultramicrotome (Reichert Jung Ultracut, Leica) at 70 nm thickness and collected on a formvar-coated single-slot nickel grid. The grids were used for anti-GABA immunogold staining and then observed in the EM. For the serial sectioning study, small blocks containing only layer I were trimmed and cut into serial ultrathin sections in ribbons and collected on single-slot copper grids. For the biocytin-filled pyramidal neurons, we first cut the blocks into 2 μm-thick semithin sections. Putative synapses were searched in the semithin sections at the light microscopic level. The semithin sections containing putative synapses were re-embedded in resin for ultramicrotomy. Serial ultrathin sections were cut and collected on copper grids, which were stained with 0.5% uranyl acetate for 30 min and 3% lead citrate for 4 min (Leica EM AC20; Leica). After contrast staining, the grids were ready for EM observation.

A transmission electron microscope (LEO 906E, Zeiss), equipped with a wide-angle dual speed 2K CCD camera (TRS; Germany), was used to take electron micrographs. We scanned layers I–Va at low magnification (×2,100) to find DAB-labeled boutons and used higher magnification (×21,000) to identify synapses. These synapses had to present three main features: (a) a cluster of synaptic vesicles close to the presynaptic membrane, (b) parallel appositions between pre- and postsynaptic membranes as well as widening of the extracellular space at the putative synaptic cleft, and (c) a postsynaptic membrane thickening, which is much thinner at the symmetric GIN bouton synapses than at asymmetric synapses. Consecutive sections were checked to verify a putative synapse, if necessary.

## 2.5 | Data analysis and statistics

The statistical analysis was carried out using libreoffice and R. The data were first tested for normal distribution (Shapiro–Wilk test). If they were normally distributed, Student's t test or one-way ANOVA followed by post hoc Tukey's HSD test was used. If they were not, Mann–Whitney *U* test or Kruskal–Wallis one-way analysis was used. If there existed a significant difference of the result of Kruskal–Wallis one-way analysis, post hoc Dunn's test with Bonferroni correction was used on pairwise multiple comparisons.

According to our previous study (Zhou et al., 2017), we used receiver operating characteristic (ROC) curve to evaluate the efficiency of anti-GABA immunogold staining and to determine the GABA immunopositivity threshold for the targets of GIN cell boutons. We sampled pyramidal neuron somata and dendritic spines as the presumable GABA-immunonegative group, and interneuron somata and interneuron dendrites as the presumable GABA-immunopositive group, and compared the gold grain density of the two groups by Mann–Whitney *U* test (Figure 6a,b). The ROC curve was generated from the two groups, using the package ROCR in R. GABA immunopositivity threshold was determined as the optimal cut-off point (closest point to (0,1)) on the ROC curve (Figure 6c).

# 3 | RESULTS

## 3.1 | Distribution of GIN cells and colocalization with somatostatin

To study the distribution and colocalization of GIN cells and SST+ interneurons, we performed anti-GFP and anti-SST double-fluorescence immunohistochemistry. We used DAPI staining to delineate cortical layers and quantified the GFP+ cells (green) and SST+ cells (red) as well as their colocalization (yellow) across layers of the barrel cortex from 24 sections of 8 GIN mice (Figure 1a). GFP+ cells were located mainly in layer II/III, accounting for 41.2% ± 10.3% (257.2 ± 77.0 cells/mm$^3$) of the total GIN cell population (648.3 ± 198.2 cells/mm$^3$). Less GIN cells were observed in layer IV with 30.7% ± 8.7% (204.8 ± 92.7 cells/mm$^3$) and in layer Va, it was 23.8% ± 6.8% (155.6 ± 67.8 cells/mm$^3$). There were few GFP+ cells in layer Vb with 4.2% ± 5.2% (29.8 ± 43.6 cells/mm$^3$) and virtually no cell was found in layers I and VI. Compared to GIN cells, SST+ cells had the highest density in layer Vb, accounting for 25.0% ± 6.8% of the total cell population (833.7 ± 414.7 cells/mm$^3$). In layers II/III, IV, Va, and VI, the proportions were 20.2% ± 6.5%, 20.2% ± 5.2%, 15.0% ± 4.6%, 19.6% ± 4.8%, respectively (layer II/III: 595.3 ± 163.0 cells/mm$^3$, layer IV: 628.2 ± 229.6 cells/mm$^3$, layer

Va: 507.0 ± 331.5 cells/mm$^3$, layer VI: 618.0 ± 224.7 cells/mm$^3$). No SST+ cell was detected in layer I. In terms of colocalization, all the GFP+ cells were also SST+ (arrowheads in Figure 1b,c) but not all SST+ cells were GFP+ (arrows in Figure 1c,d). The layer-associated distribution of the colocalization was quantified: in total GFP+ cells accounted for 21.3% ± 4.9% of SST+ interneurons, with 44.4% ± 6.1% in layer II/III, 32.0% ± 5.9% in layer IV, 35.2% ± 9.9% in layer Va and 3.5% ± 4.5% in layer Vb (Figure 1e). Thus, the colocalization study shows that the GIN mouse labels a fraction of SST+ interneurons, preferentially the ones in layers II–Va of the barrel cortex.

## 3.2 | Colocalization of GIN cells and with calretinin

To further characterize the neurochemical profile of GIN cells, we performed anti-GFP and anti-CR double immunostaining and analyzed the colocalization of GIN cells and CR+ interneurons in layers II/III–V (Figure 2a,a'). The CR+ interneuron density was almost three times higher than the GIN cells (CR+ cells: 2502.3 ± 338.0 cells/mm$^3$, GFP+ cells: 849.7 ± 114.7 cells/mm$^3$). 54.1% ± 5.9% of the CR+ interneurons located in layer II/III (1344.1 ± 255.8 cells/mm$^3$). There was 3.5% ± 0.9% in layer 1 (83.8 ± 37.0 cells/mm$^3$), 20.4% ± 3.9% in layer IV (517.6 ± 93.8 cells/mm$^3$), 8.5% ± 0.9% in layer Va (214.4 ± 74.8 cells/mm$^3$), and 6.0% ± 1.3% in layer Vb (149.2 ± 51.1 cells/mm$^3$), 7.6% ± 0.6% in layer VI (189.2 ± 61.3 cells/mm$^3$). Most of the GFP+ cells, which were immunopositive for CR, were found in layer II/III (Figure 2b,c). In the other layers, GFP+ cells were more likely to be CR-immunonegative (Figure 2d,e). The colocalization ratio was analyzed across layers (Figure 2a'): in total, it was 29.0% ± 7.2%, with 53.9% ± 14.9% in layer II/III, 8.3% ± 10.4% in layer IV, 10.6% ± 8.4% in layer Va and 23.1% ± 33.6% in layer Vb. Consistent with a previous study (Xu et al., 2006), we found nearly one-third of GIN cells coexpress CR in the mouse barrel cortex, and the colocalization rate is relatively high in layer II/III and much lower in layers IV and V. However, we did not find any obvious relationship between colocalization and somatodendritic morphology of the double-labeled neurons.

## 3.3 | GIN cells have distinct somatodendritic configurations

As shown in Figure 2b–e, the subtypes of GIN cells displayed diverse somatodendritic morphologies. In order to study the morphological diversity of GIN cells, we used anti-GFP DAB-peroxidase staining to visualize the cells in a Golgi-like manner. The distribution of GIN cells in this brightfield approach (Figure 3a) was virtually identical with the pattern observed by anti-GFP immunofluorescence (Figure 1a). Previous studies indicated that Martinotti cells have multipolar or bitufted somatodendritic configurations (Kawaguchi & Kondo, 2002; Kawaguchi & Kubota, 1996; Wang et al., 2004). We found that GIN cells are sparsely spiny neurons and most of them had typical multipolar somatodendritic morphology, with a round soma from which four to eight primary dendrites extended horizontally in all directions (Figure 3b-a). Multipolar GIN cells could be both, CR+ (Figure 2b,b') and CR– (Figure 2d,d'). There were also tufted neurons with an oval or

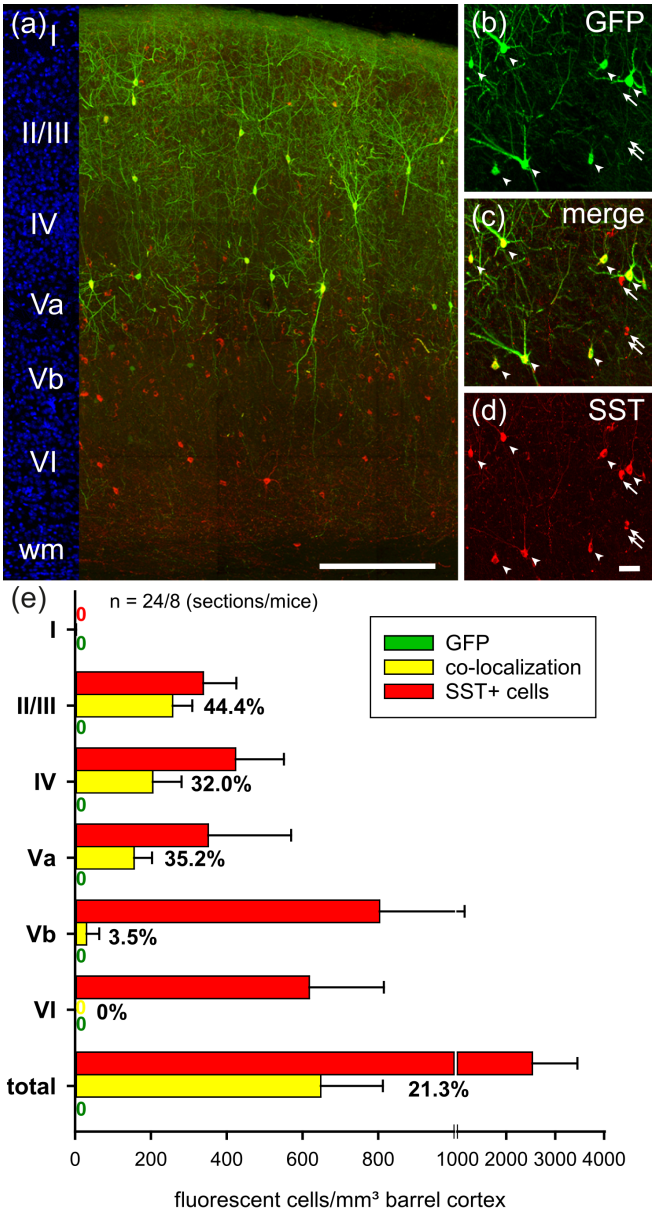


**FIGURE 1** Distribution of GIN cells and colocalization with SST-immunoreactivity (+) in the barrel cortex of GFP-expressing transgenic mice. (a) Anti-GFP and anti-SST immunostaining shows GIN cells (green) and SST+ neurons (red) in the barrel cortex. DAPI staining (blue) reveals cortical layers I to VI. (b–d) Colocalization of GFP+ cells and anti-SST immunopositive (SST+) neurons. Please note that all GIN cells colocalize with SST+ (arrowheads in b–d) but not all SST+ neurons express GFP (arrows in c–d). (e) Distribution of SST+ neurons (red), double-labeled SST+/GFP+ neurons (yellow) and only GFP+ neurons (non-SST expressing cells) (green) across layers of the barrel cortex. The analysis derives from 24 sections out of 8 animals and is presented as cells/mm$^3$ (mean, error bar = SD). The ratio of GIN cells to SST+ neurons in each layer is shown next to yellow bars (mean). Scale bars: (a) 200 μm; (b–d) 50 μm. GIN, GFP-expressing inhibitory neurons; SST+, Somatostatin-expressing

fusiform soma, from which the dendrites extended in a more vertically biased orientation (Figure 3b, f', d). The tufted neurons also could be both CR+ (Figure 2c,c') and CR– (Figure 2e,e'). As a rare case, a locally

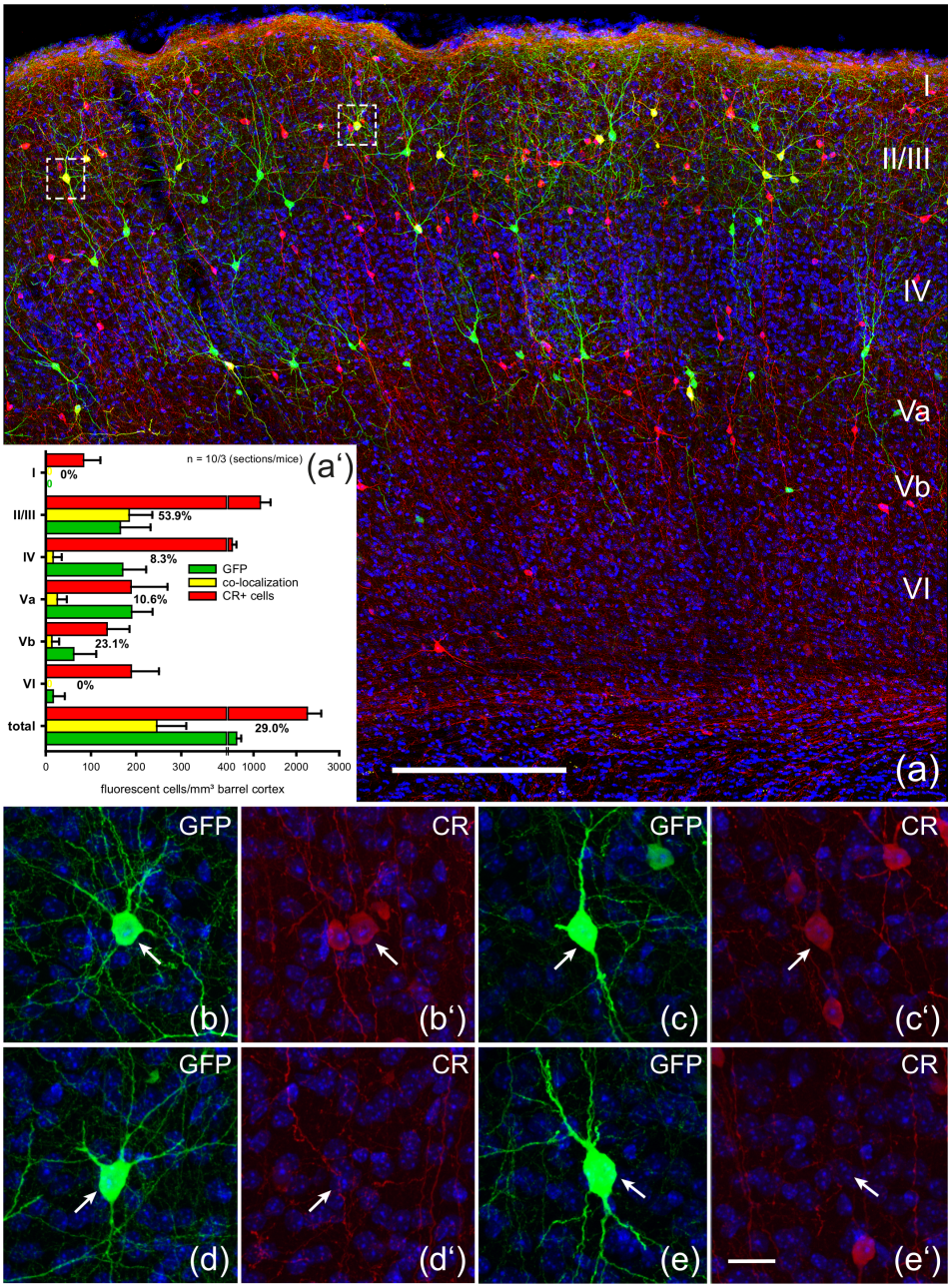


**FIGURE 2** Distribution of GIN cells and colocalization with calretinin-immunoreactivity (CR+) in the barrel cortex of GFP-expressing transgenic mice. (a) Anti-GFP and anti-CR immunostaining shows GIN cells (green) and CR+ neurons (red) in the barrel cortex. DAPI staining reveals cortical layers I to VI. (a') Distribution of CR+ neurons (red), double-labeled CR+/GFP+ neurons (yellow) and GFP+ neurons (green) across layers of the barrel cortex. The analysis derives from 10 sections out of 3 animals and is summarized as cells/mm$^3$ (mean, error bar = SD). The ratio of GIN cells to CR+ neurons in each layer is shown next to yellow bars (mean). (b,b') Colocalization of GFP and CR in a layer II/III multipolar GIN cell (indicated by right square in a). (c,c') Colocalization of GFP and CR in a layer II/III modified bipolar GIN cell (indicated by left square in a). (d,d') Lack of colocalization of GFP and CR in a layer II/III multipolar GIN cell (not shown in a). (e,e') Lack of colocalization of GFP and CR in a layer II/III modified single tufted GIN cell (not shown in a). Scale bar: (a) 250 μm; (b–e) 25 μm. GIN, GFP-expressing inhibitory neurons; SST+, Somatostatin-expressing

projecting non-Martinotti cell at the layer IV/Va border was identified by virtue of its very dense axonal arbor just above the soma in layer IV (Figure 3a, white arrow and asterisk, Figure 3c).

To quantitatively analyze the somatodendritic configurations, we sampled 147 GIN cells from layers II to V of the barrel cortex (three mice, nine sections). The cell bodies located within the sections and the primary dendritic processes were not severed to any visible extent. According to the previous classification criteria (Cauli, Zhou, Tricoire, Toussay, & Staiger, 2014), we classified the 147 GIN cells into nine subtypes, as shown by the somatodendritic reconstructions (Figure 3d). In total, there were 50.3% multipolar cells (a), 4.8% tripolar cells (b), 4.1% horizontal cells (c), 4.1% bitufted cells (d), 2.7% modified bitufted (e), 7.5% single tufted cells (f', f''), 13.6% modified single tufted cells (g', g''), 2.0% bipolar cells (h) and 10.9% modified bipolar cells (i). The nine somatodendritic subtypes can be found throughout all examined layers, but there were layer-dependent preferences (Table 1). For multipolar cells, layers IV and V showed lower ratios than layer II/III (layer II/III 59.3%, layer IV 47.4%, and layer V 36.7%). In contrast, the proportion of modified cells (including modified single tufted and modified bipolar cells) was higher in layers IV and V than in layer II/III (layer II/III 16.9%, layer IV 33.3%, and layer V 36.7%). Finally, as the minority, tripolar cells had a higher ratio in layer V compared to layers II/III and IV (layer II/III 3.4%, layer IV 1.8%, and layer V 13.3%). For the remaining somatodendritic subtypes, the ratios were similar across layers.

In addition to somatodendritic morphology, the origin of the axons was analyzed in 107 GIN cells. The axons originated either from the upper pole/side of the soma or from an ascending primary or

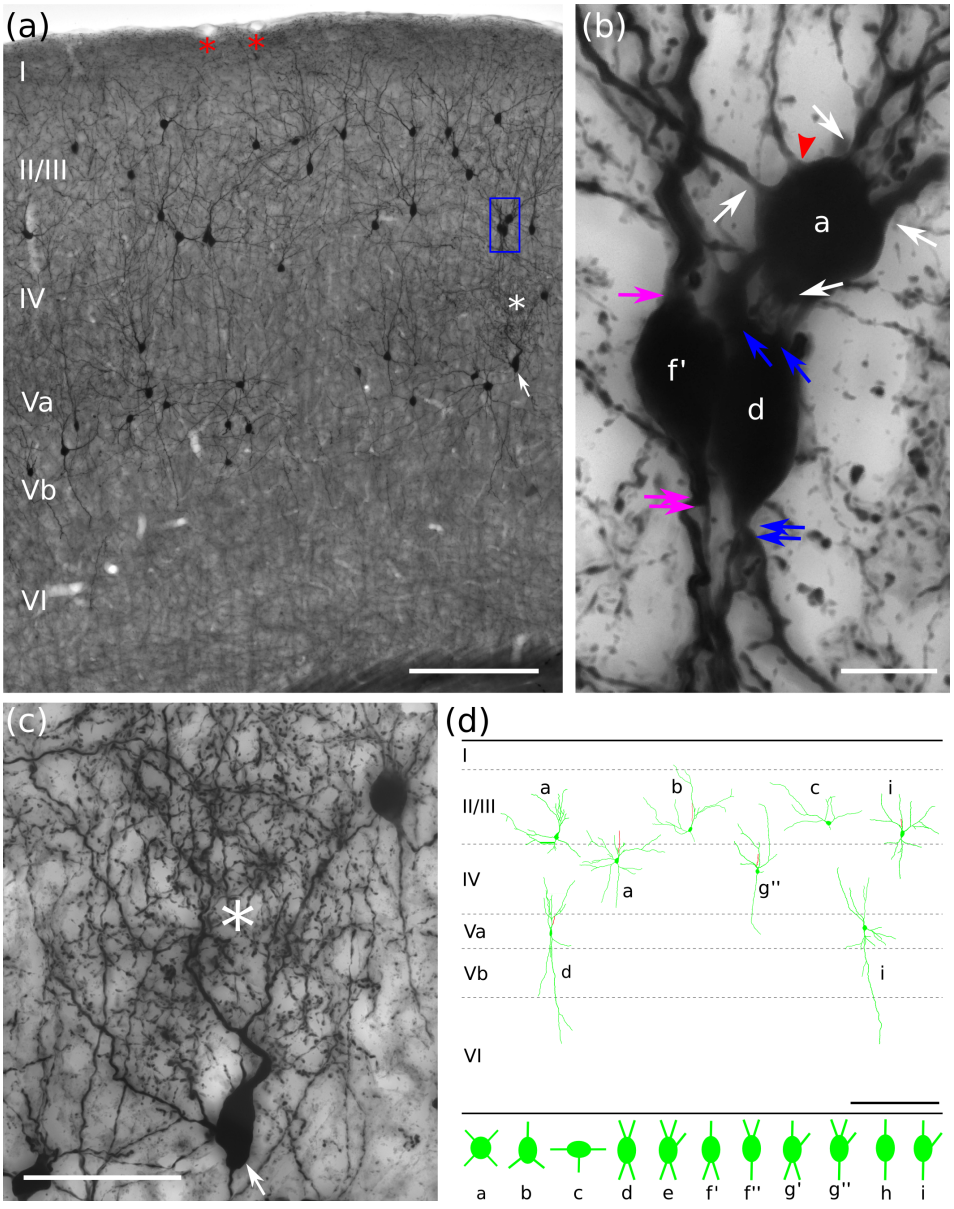


**FIGURE 3** Somatodendritic morphology of GIN cells in the barrel cortex of GFP-expressing transgenic mice. (a) DAB-peroxidase staining shows the distribution and Golgi-like morphology of GIN cells. Martinotti cells can be found mainly in layer II/III and more rarely in layers IV and Va. As a rare exception, a non-Martinotti cell at the layer IV/Va-border is recognizable (white arrow) due to its profuse local axonal arbor (white asterisk). Red asterisks mark the region of the pial surface containing blood vessels. (b) Typical morphology of Martinotti cells in layer II/III (blue inset in a). The multipolar neuron (a) has four primary dendrites (white arrows). Its axon originates from the soma and ascends toward layer I (red arrowhead). The bitufted neuron (d) possesses two primary dendrites in each tuft (blue arrows). The single tufted neuron (f') shows a single dendrite (toward the pia) and two dendrites (toward the white matter; pink arrows). (c) the non-Martinotti cell at the layer IV/Va-border is shown in high resolution. The axon arborizes intensively in layer IV and is restrict to a single barrel column (white asterisk). (d) Reconstruction of the somatodendritic morphology (green; red is the axon initial segment) and classification of the somatodendritic configurations of GIN cells. (a) Multipolar, (b) tripolar, (c) horizontal, (d) bitufted, (e) modified bitufted, (f',f'') single tufted, (g',g'') modified single tufted, (h) bipolar, (i) modified bipolar. Scale bars: (a) 200 μm; (b) 10 μm; (c) 50 μm; (d) 250 μm. GIN, GFP-expressing inhibitory neurons; SST+, Somatostatin-expressing

secondary dendrite. All the axons extended radially toward layer I. Because of the population staining approach, it was difficult to trace the axons and reconstruct the axonal distribution. However, it was interesting to note that the origin of the axons was significantly correlated with the somatodendritic morphology ($\chi^2$ = 15.2, $df$ = 8, $p$ = .049). In particular, the multipolar cells had more soma-deriving axons, while the modified cells as well as single tufted and bitufted neurons were more likely to have axons originating from ascending dendrites (Table 1). In summary, GIN cells, mainly represented by multipolar neurons, have diverse somatodendritic configurations, which is a morphological feature that strongly correlates with the axon origin. The different somatodendritic subtypes co-exist throughout the analyzed

**TABLE 1** Distributions of different somatodendritic subtypes and their axon origin

| | Layers | | | | Axon origin | | |
|---|---|---|---|---|---|---|---|
| Somatodendritic subytpes | *n* | LII/III (%) | LIV (%) | LVa-b (%) | *n* | From dendrite (%) | From soma (%) |
| Multipolar | 74 | 59.3 | 47.4 | 36.7 | 59 | 45.8 | 54.2% |
| Tripolar | 7 | 3.4 | 1.8 | 13.3 | 5 | 60.0 | 40.0 |
| Horizontal | 6 | 3.4 | 3.5 | 6.7 | 3 | 0.0 | 100.0 |
| Bitufted | 6 | 5.1 | 5.3 | 3.3 | 5 | 80.0 | 20.0% |
| Modified-bitufted | 4 | 3.4 | 0.0 | 6.7 | 1 | 0.0 | 100.0 |
| Bipolar | 3 | 3.4 | 1.8 | 0.0 | 2 | 50.0 | 50.0 |
| Modified-bipolar | 16 | 5.1 | 14.0 | 16.7 | 10 | 80.0 | 20.0 |
| Single tufted | 11 | 8.5 | 7.0 | 3.3 | 5 | 100.0 | 0.0 |
| Modified-singletufted | 20 | 8.5 | 19.3 | 13.3 | 17 | 64.7 | 35.3 |
| Total | 147 | 100.0 | 100.0 | 100.0 | 107 | 55.1 | 44.9 |

layers of the barrel cortex and the distributions seem to be layer specific.

## 3.4 | The axonal distribution and synaptic ultrastructure of GIN cells

According to their assumed identity as Martinotti cells, GIN cell axons strongly innervated layer I and formed extensive arborizations there, especially in the upper layer I (Figure 4a). The density of the axonal innervation gradually decreased in layers II/III, IV, and Va (Figure 4b). The bouton density was 14.35 ± 4.15 boutons/(10 μm)$^3$ in layer I, 5.09 ± 2.01 boutons/(10 μm)$^3$ in layer II/III, 3.59 ± 1.49 boutons/(10 μm)$^3$ in layer IV, and 1.88 ± 0.25 boutons/(10 μm)$^3$ in layer Va (mean ± SD). The bouton density of layer I was significantly higher than in the other layers, and there was no significant difference among the other layers (one-way ANOVA, $F = 15.84$, $df = 3$, $p < .001$, post hoc Tukey's HSD, Figure 4c). Only few axonal collaterals entered into layers Vb and VI, and thus the bouton density was not quantified there.

In order to study the axonal and synaptic ultrastructure, we traced single axons in layer I in serial sections and analyzed their geometry as well as bouton/synapse ratio. We found that GIN cell axons very often formed small boutons containing no mitochondria, which made synaptic junctions with their target structures (Figure 5a–d, b1). Presynaptic boutons containing mitochondria were larger and also formed larger synaptic junctions (Figure 5a–d, b2). We traced 17 presynaptic profiles in serial sections: all of them formed symmetric synapses with dendritic shafts; 52.9% (9/17) of the presynaptic profiles were small boutons without mitochondria, and 47.1% (8/17) were large boutons with mitochondria. Most of the boutons formed only one synaptic junction with one target structure, and only one bouton was found to form two synaptic junctions with two different target structures. Interestingly, we occasionally found two synapses of a single GIN cell axon clustering onto the same target, for example, a larger-caliber dendritic shaft in layer I (Figure 5a–d).

As synaptic strength is closely related to presynaptic and postsynaptic ultrastructural features (Holderith et al., 2012; Kubota & Kawaguchi, 2000; Rollenhagen et al., 2015), we quantified the size of presynaptic boutons and postsynaptic density (PSD) in cross sections, in a layer-specific manner. In total, we sampled 185 GIN cell synapses from cortical layers I to Va (layer I: $n = 102$, layer II/III: $n = 38$, layer IV: $n = 29$, layer Va = 16). To compare the GIN cell synapses with the ones of VIP+ cells, we used the data set of our previous study and re-sampled 96 VIP+ cell synapses from layers I to V (Zhou et al., 2017) (layer I: $n = 8$, layer II/III: $n = 44$, layer IV: $n = 25$, layer V: $n = 19$). There was no layer-dependent difference in the size of presynaptic boutons and PSD of both GIN cell and VIP+ cell synapses, and thus the data sets of each layer were pooled together. We found the distribution of GIN presynaptic boutons was unimodal, which suggests that the large and small boutons are from the same types of GIN cells (Figure 5e). Compared to the VIP+ presynaptic boutons (Figure 5f), boutons of GIN cells were significantly smaller (GIN cells: 0.02–0.68 μm$^2$; VIP+ cells: 0.09–1.10 μm$^2$; Mann-Whitney $U$ test, $U = 3{,}927$, $p < .001$). In addition, the PSD length measured in single cross sections of postsynaptic profiles opposed to GIN boutons were significantly shorter than the ones opposed to VIP+ boutons (GIN boutons: 0.09–0.45 μm; VIP+ boutons: 0.14–0.66 μm) (Figure 5g, Mann-Whitney $U$ test, $U = 5218$, $p < .001$). The correlation coefficient (r) of PSD length and bouton size was measured in both types of synapses: a weaker correlation was found in GIN cells ($r = .18$) compared to VIP cells ($r = .39$) (Figure 5g). In addition, the results indicate that GIN cell axons have unique ultrastructural features, mainly characterized by small presynaptic boutons that innervate their targets via small synaptic junctions.

## 3.5 | Synaptic innervation of subcellular target structures by GIN cell boutons

In total, we sampled 249 GIN cell synapses from layers I to Va (layer I: $n = 119$, layer II/III: $n = 56$, layer IV: $n = 47$, layer Va: $n = 27$). They were formed by 238 boutons, as there were nine boutons forming

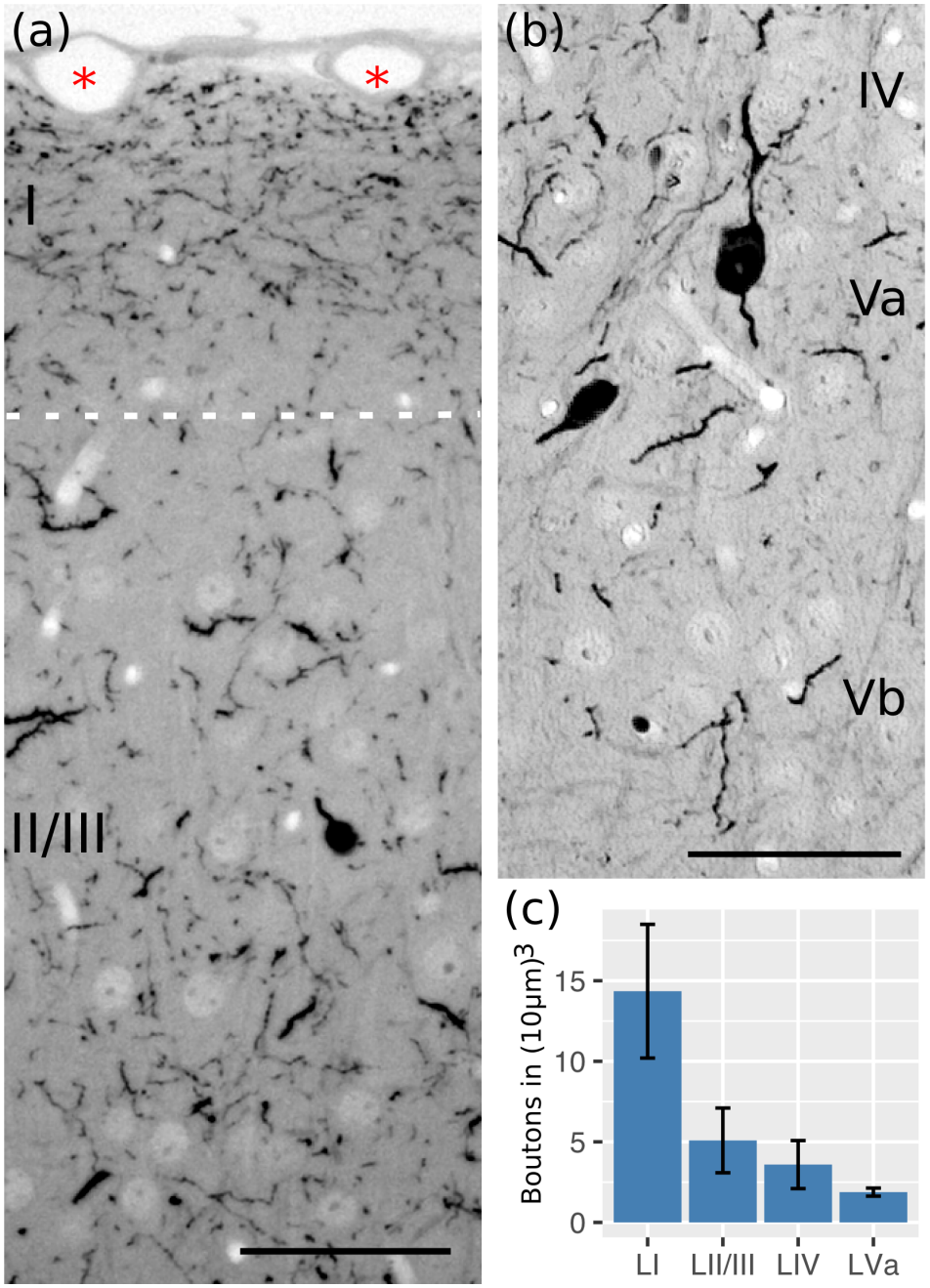


**FIGURE 4** Quantification of axonal boutons of GIN cells across layers. (a,b) Light microscopic images of 2 µm-thick semithin sections show the gradient of axonal innervation being densest in layer I (a, top), less in layer II/III (a, bottom), and least in deeper layers IV to Vb (b). Asterisks indicate the region corresponding to Figure 3a. (c) Quantification of the bouton density from layers I to Va. The analysis derives from three GIN mice and is presented as boutons/(10 µm)$^3$ in mean ± SD (error bar). Layer I has a significantly higher bouton density compared to layers II/III, IV, and Va (one-way ANOVA, $F = 15.84$, $df = 3$, $p < .001$, pairwise post hoc Tukey's test). Scale bars: (a,b) 50 µm. ANOVA, analysis of variance; GIN, GFP-expressing inhibitory neurons

two synapses and one bouton forming even three synapses. Dendrites represented 88.4% (220/249) of the postsynaptic structures, whereas only 11.6% (29/249) of the targets were dendritic spines. We neither found somatic synapses of GIN boutons nor synapses with any subcellular compartment of GIN cells themselves. The ratio of synapses innervating dendritic shafts versus spines did not significantly differ across layers: the dendrite-targeting synapses accounted for 88.2% (105/119) in layer I, 89.3% (50/56) in layer II/III, 87.2% (41/47) in layer IV, and 88.9% (24/27) in layer Va (Table 2).

In order to quantify the connectivity of GIN cells with excitatory versus inhibitory neurons, we used post-embedding anti-GABA immunogold staining to label GABAergic subcellular profiles. For that purpose, we first evaluated the specificity and sensitivity of the anti-GABA immunogold staining by comparing the gold grain density of presumably GABA-immunopositive and GABA-immunonegative profiles (Figure 6a,b). Then, we generated the ROC curve from positive and negative labelings and used the ROC curve to determine a threshold for GABAergic dendrites, which was found to be 7.2 gold grains/µm$^2$ (Figure 6c).

Altogether, we analyzed 188 dendrites from layers I to Va (layer I: $n = 90$, layer II/III: $n = 45$, layer IV: $n = 30$, layer Va: $n = 23$). Of these, 90% (170/188) were GABA-negative without any or with only few gold grains (Figure 7a–c). The large dendrite in layer I (Figure 7a) is very likely to belong to the tuft of a pyramidal neuron according to its unique ultrastructure (Peters, Palay, & Webster, 1991). The GABA-negative ratio was similar across layers: 93% (84/90) in layer I, 89% (40/45) in layer II/III, and 87% (LIV: 26/30, LVa: 20/23) in layers IV

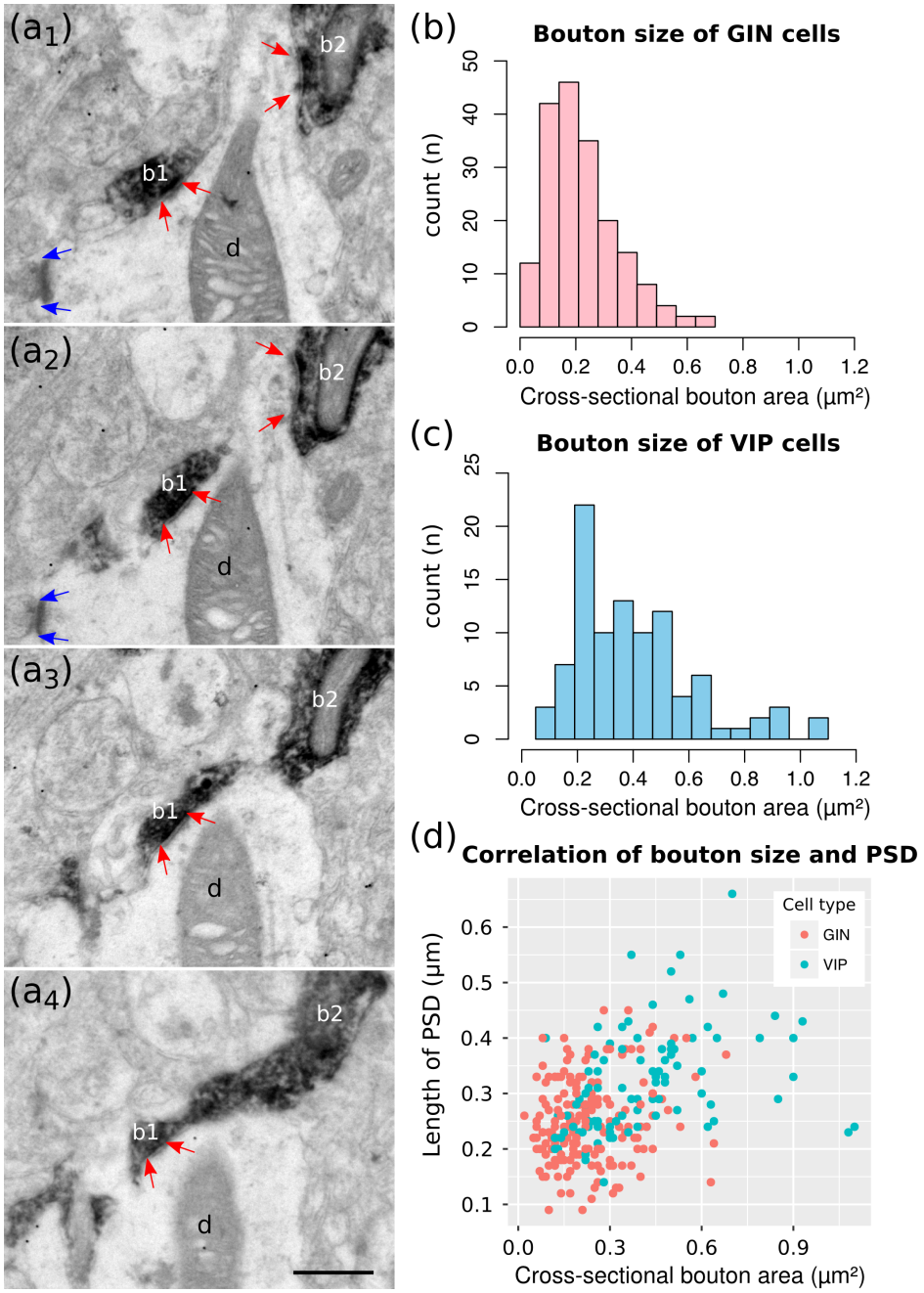


**FIGURE 5** Qualitative and quantitative analysis of ultrastructural features of GIN cell synapses. ($a_1$–$a_4$) A larger-caliber dendritic shaft (d) in layer I receives two symmetric synapses formed by two boutons (b1, b2) of a single GIN cell axon. Red arrows: Symmetric synapse. Blue arrows: Asymmetric synapse. (b,c) Histograms of the cross-sectional area ($\mu m^2$) of presynaptic boutons of GIN cells (b) and VIP+ cells (c). Synapses of GIN cells and VIP cells were sampled from layers I to V (GIN cells: in total, $n$ = 185, layer I: $n$ = 102, layer II/III: $n$ = 38, layer IV: $n$ = 29, layer Va: $n$ = 16; VIP+ cells: in total, $n$ = 96, layer I: $n$ = 8, layer II/III: $n$ = 44, layer IV: $n$ = 25, layer V: $n$ = 19). To avoid the skewness of the samples, the data sets of each layer were pooled. Boutons of GIN cells were significantly smaller than VIP+ cells (Mann–Whitney $U$ test, $U$ = 3,927, $p$ < .001). (d) PSD of GIN cells is significantly smaller than that of VIP+ cells (Mann–Whitney $U$ test, $U$ = 5,218, $p$ < .001). The correlation coefficient (r) indicates a weak correlation of PSD to bouton size in VIP cells ($r$ = .39) and nearly no correlation in GIN cells ($r$ = .18). Scale bar: ($a_1$–$a_4$) 0.5 µm. PSD, postsynaptic density; GIN, GFP-expressing inhibitory neurons; VIP+, vasoactive intestinal polypeptide-expressing

and Va. None of the innervated spines was GABA-positive. It should be noted that 69% (20/29) of the innervated spines also received excitatory synapses in the vicinity of GIN cell synapses (Figure 7d).

Compared to VIP+ interneurons (Zhou et al., 2017), GIN cells rarely targeted GABAergic inhibitory cell dendrites, as identified by GABA immunogold labeling (Figure 7e,f). The innervated GABAergic dendrites were often found to additionally receive several excitatory synapses in the vicinity of GIN cell synapses (Figure 7e). Overall, only 10% (18/188) of the targeted dendrites were GABA-positive and the ratio was similar across layers (layer I: 7%, 6/90; layer II/III: 11%, 5/45; layer IV: 13%, 4/30; layer Va: 13%, 3/23). In addition, there was also no layer-specific difference in terms of GABA labeling density of the targeted dendrites (Figure 8). Interestingly, the innervated dendrites in layer I were significantly larger in diameter compared with the ones in the other layers, the other layers, however, not showing significant differences (Figure 8, Kruskal–Wallis test, $H$ = 48.6, $df$ = 3, $p$ < .001, Post hoc Dunn's test with Bonferroni correction). The large dendrites in layer I are likely to belong to tufts at the distal end of the apical dendrite of pyramidal neurons. Taken together, the ultrastructural study on the postsynaptic innervation of GIN boutons indicates that GIN cells are preferentially dendrite-targeting interneurons, and that they primarily innervate dendrites of excitatory neurons without layer-specific differences, in agreement with our assumption that GIN cells are mainly Martinotti cells, at least outside layer IV.

As our quantitative study indicates, GIN cells preferentially target pyramidal neurons at their distal apical dendritic shafts. We performed

a proof-of-principle experiment for the innervation of a single biocytin-filled pyramidal neuron by GIN cell boutons, using correlated light and electron microscopy (Figure 9). GIN mouse brain slices were used and whole-cell patch-clamp recordings were carried out. A pyramidal neuron in layer II/III of the barrel cortex was recorded and filled with biocytin. The morphology of the neuron was successfully recovered and visualized by streptavidin-peroxidase/DAB staining (Figure 9a). After imaging, we did anti-GFP immunostaining to visualize the GIN cells and their boutons. The immunohistochemistry reached a penetration of around 60 μm in the slice and GIN cell boutons showed up in layer I in semithin sections (Figure 9c). Since the biocytin-filled pyramidal neuron and GIN cells were both stained by DAB in black, we could not differentiate dendritic spines and putative boutons of GIN cells in semithin sections. Therefore, we correlated each semithin section (27 sections covering 54 μm in z) with the original image stack of the pyramidal neuron. The black dots, which were located in close vicinity of the dendritic segments of pyramidal neuron in semithin sections and did not show up as spines in the original image stack, were considered as putative presynaptic boutons. In total, 17 putative boutons were found and 15 of them were onto two different distal apical dendritic branches, whereas only two putative boutons were found at the basal dendrites (Figure 9b).

To confirm this light microscopic observation of putative synapses of GIN cells, we focused on one GIN cell bouton at one of the apical dendritic tufts (b1 in the insets of Figure 9b–d). We performed serial ultrathin sectioning and found the apical dendritic tuft as well as the bouton, as shown by the low magnification electron micrograph (b1 in the inset of Figure 9d). The high magnification electron micrographs of nonadjacent serial sections show synaptic vesicles in the bouton, a

**TABLE 2** Distribution of subcellular target structures across layers

| Layers | *n* | Dendrite | Spine | Dendrite (%) | Spine (%) |
|---|---|---|---|---|---|
| LI | 119 | 105 | 14 | 88.2 | 11.8 |
| LII/III | 56 | 50 | 6 | 89.3 | 10.7 |
| LIV | 47 | 41 | 6 | 87.2 | 12.8 |
| LVa | 27 | 24 | 3 | 88.9 | 11.1 |
| All | 249 | 220 | 29 | 88.4 | 11.6 |

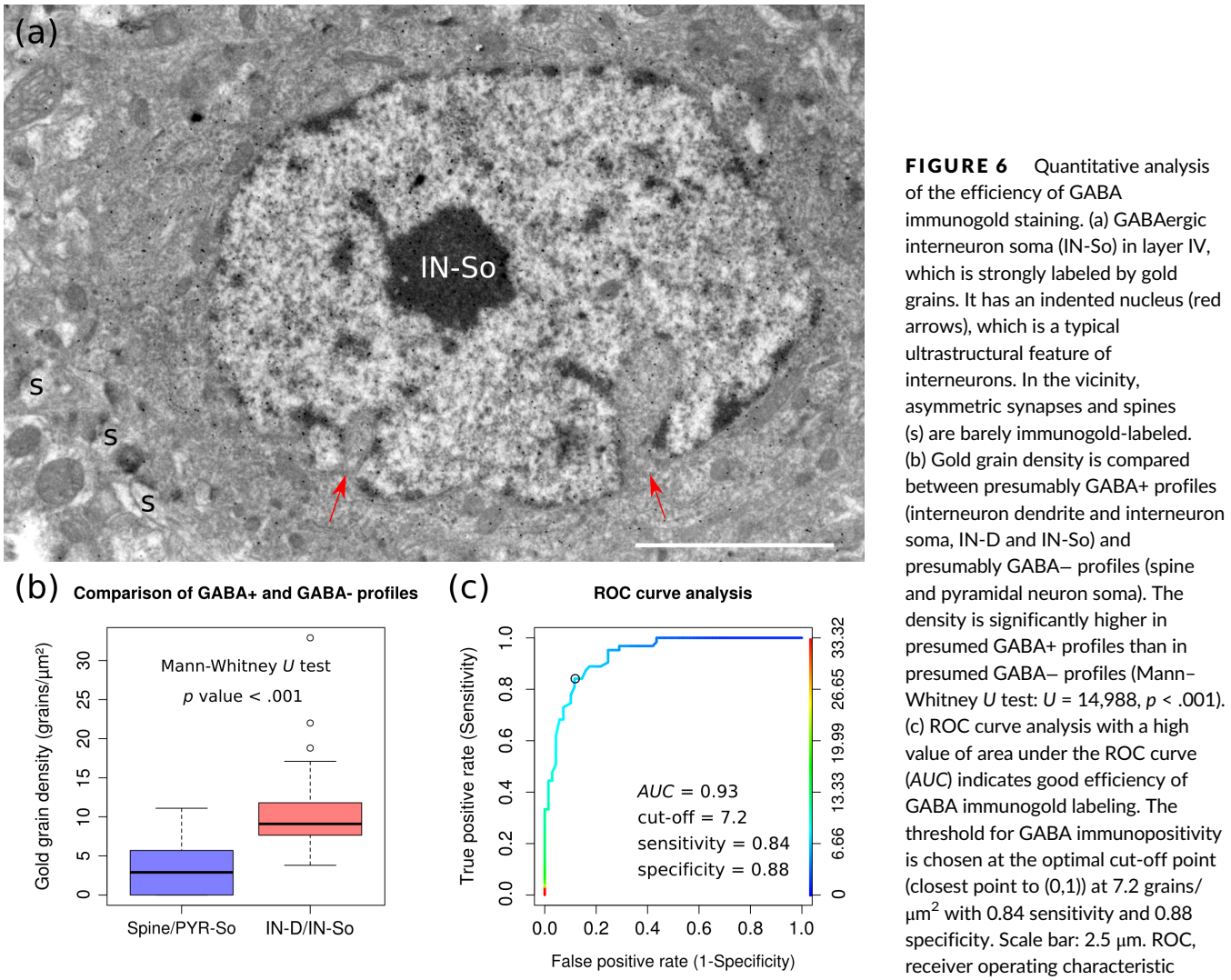


**FIGURE 6** Quantitative analysis of the efficiency of GABA immunogold staining. (a) GABAergic interneuron soma (IN-So) in layer IV, which is strongly labeled by gold grains. It has an indented nucleus (red arrows), which is a typical ultrastructural feature of interneurons. In the vicinity, asymmetric synapses and spines (s) are barely immunogold-labeled. (b) Gold grain density is compared between presumably GABA+ profiles (interneuron dendrite and interneuron soma, IN-D and IN-So) and presumably GABA– profiles (spine and pyramidal neuron soma). The density is significantly higher in presumed GABA+ profiles than in presumed GABA– profiles (Mann–Whitney *U* test: $U = 14{,}988$, $p < .001$). (c) ROC curve analysis with a high value of area under the ROC curve (*AUC*) indicates good efficiency of GABA immunogold labeling. The threshold for GABA immunopositivity is chosen at the optimal cut-off point (closest point to (0,1)) at 7.2 grains/$\mu m^2$ with 0.84 sensitivity and 0.88 specificity. Scale bar: 2.5 μm. ROC, receiver operating characteristic

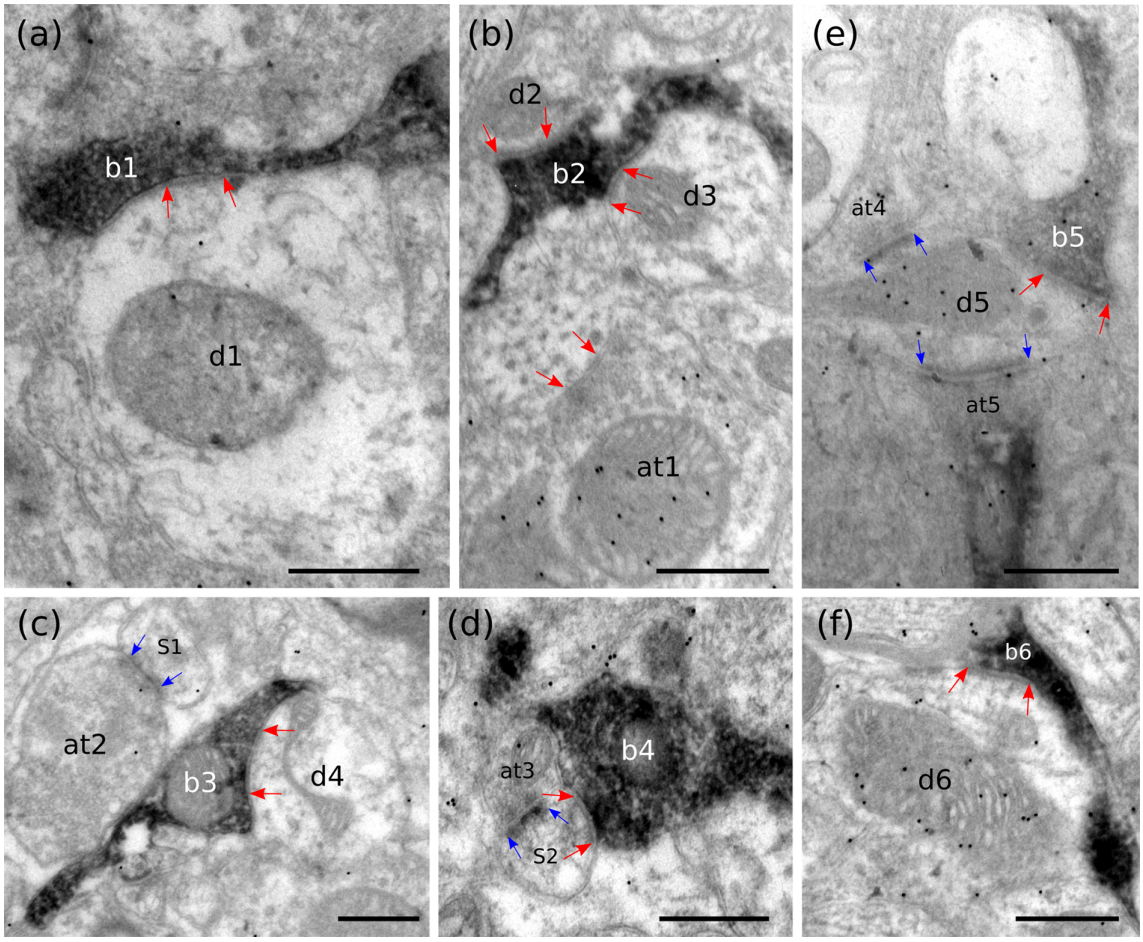


**FIGURE 7** GIN cell boutons preferentially target non-GABAergic subcellular profiles but rarely synapse with GABAergic profiles. (a) GIN cell bouton in layer I (b1) innervates a thick dendritic shaft, which is GABA immunonegative (d1). (b) GIN cell bouton (b2) targets two non-GABAergic dendrites (d2, d3) in layer II/III. In contrast, a symmetric synapse is strongly labeled by gold grains on the presynaptic terminal (at1). (c) A large Bouton (b3) in layer IV contacts a GABA− dendrite (d4). A neighboring asymmetric synapse formed by an axonal terminal (at2) and a dendritic spine (s1) is also GABA−. (d) Another large Bouton (b4) in layer Va contacts a spine (s2), which is also innervated by a small asymmetric axonal terminal (at3). (e) GIN cell bouton in layer I (b5) innervates a GABA+ dendrite (d5), which also receives asymmetric synaptic input from two GABA − axonal terminals (at4, at5). (f) Small diameter increase of a GIN axon in layer Va (b6) that synapses on a GABA+ dendrite (d6). Red arrows: Symmetric synapse. Blue arrows: Asymmetric synapse. Scale bars: (a–f) 0.5 μm. GIN, GFP-expressing inhibitory neurons

synaptic cleft and the darkening of the PSD on the dendritic tuft ($d_{pyr}$) (Figure 9e,f). Thus, by using correlated light and electron microscopy, we confirmed the synaptic innervation of GIN cells onto pyramidal neurons, preferentially at the distal apical dendrites and apical dendritic tufts.

## 4 | DISCUSSION

In the neocortex, the GFP-expressing neurons in GIN mice initially have been considered to be mainly Martinotti cells (Ma et al., 2006; Oliva et al., 2000). However, recent studies suggested that GIN cells might be more diverse in their morphology, electrophysiology, and molecular identity in the various cortical regions than previously thought (Halabisky et al., 2006; McGarry et al., 2010; Riedemann et al., 2018; Scala et al., 2018; Xu et al., 2006). In our study, we characterized GIN cells at a population level in terms of their neurochemical specificity, somatodendritic morphology, axonal ultrastructure as well as synaptic innervation pattern. We showed that GIN cells represent a sizeable subpopulation of SST+ interneurons in layers II–Va and have diverse somatodendritic configurations across layers. They coexpressed CR with varying ratios from layers II/III to V. They formed small synapses mainly onto dendritic shafts, which were preferentially distal apical dendrites and dendritic tufts of pyramidal neurons and rarely dendrites of GABAergic interneurons. We conclude that although GIN cells show diverse morphology, they form a rather uniform inhibitory circuit motif by nearly exclusively innervating the dendrites of excitatory neurons.

### 4.1 | Multimodal characterization of GIN cells

Our study showed that GIN cells all belong to the SST+ interneuron subpopulation of GABAergic neurons in mouse barrel cortex. In

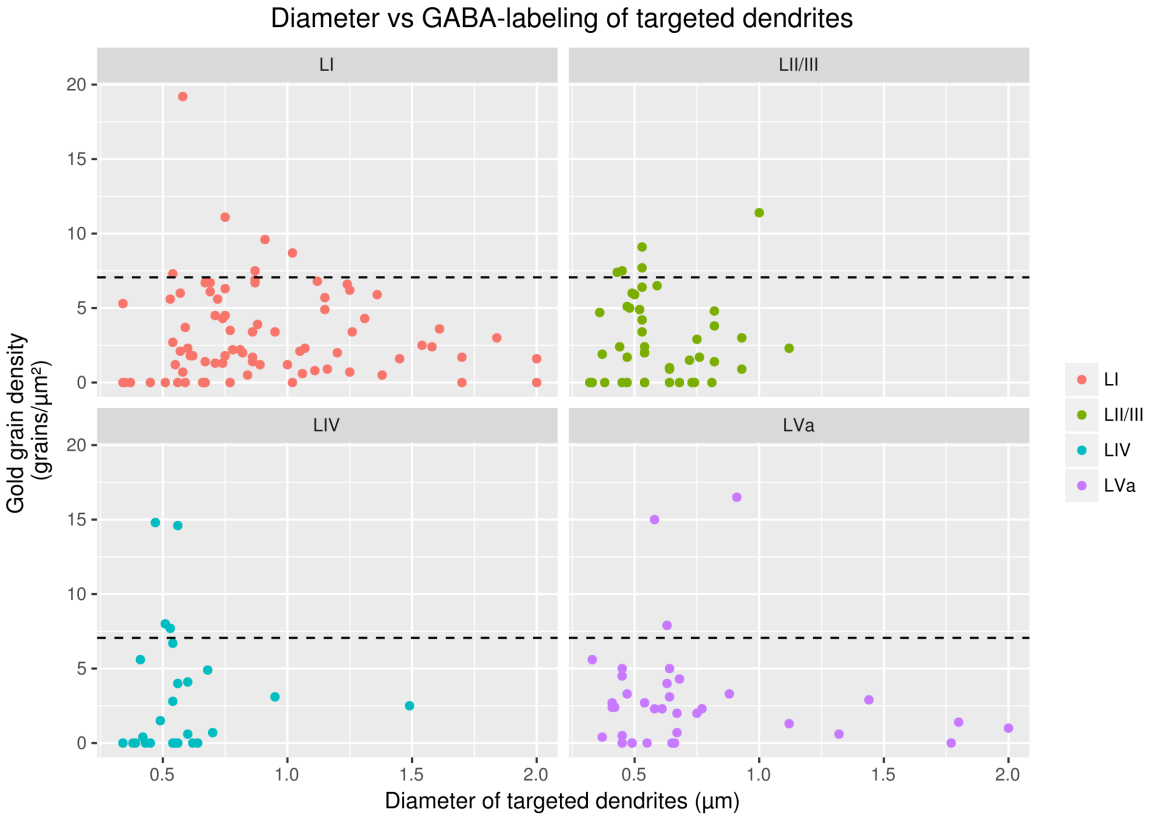


**FIGURE 8** Distribution of GABA-labeling density (grains/$\mu m^2$) with respect to cross-sectional area ($\mu m^2$) of targeted dendrites. Subcellular target structures were sampled throughout layers I to Va (total $n$ = 188, layer I: $n$ = 90, layer II/III: $n$ = 45, layer IV: $n$ = 30, layer Va: $n$ = 23). The GABA immunopositivity threshold is indicated as dashed lines. There are very few dendrites with a density above threshold (7.2 grains/$\mu m^2$), which shows no layer-dependency. There is a layer-dependent difference in the diameter of targeted dendrites as shown by Kruskal–Wallis one-way analysis ($H$ = 48.6, $df$ = 3, $p$ < .001). Post hoc pairwise comparison shows more dendrites in layer I to have a large caliber than the ones in the other layers (Dunn's test with Bonferroni correction: layer I vs. layer II/III, $p$ < .001; layer I vs. layer IV, $p$ < .001; layer I vs. layer Va, $p$ = .002)

addition, our reconstruction and refined analysis of the somatodendritic morphology indicates morphologically diverse subtypes of GIN cells throughout layers II–V. Riedemann et al. (2018) analyzed the morphology of the GIN cells in layer II/III of mouse cingulate cortex and showed the distribution of various somatodendritic subtypes, with 46% multipolar cells, 8% tripolar cells, 2% bipolar cells, 19% single tufted, 12% bitufted, 11% modified single- or bitufted, and 7% unclassified. We also found a similar distribution of the diverse somatodendritic subtypes in mouse barrel cortex with multipolar neurons being the majority. It is unknown how these diverse somatodendritic subtypes correlate with the diversity of GIN cells, as suggested by previous single cell studies (Halabisky et al., 2006; McGarry et al., 2010). However, multipolar and bitufted neurons might represent Martinotti cells according to the previous morphological studies (Kawaguchi & Kondo, 2002; Kawaguchi & Kubota, 1996; Wang et al., 2004). Nevertheless, it is interesting to observe decreased ratios of multipolar GIN cells and increased ratios of modified GIN cells in layers IV–V compared to layer II/III.

The differential distribution of these somatodendritic subtypes suggests that there could be layer-specific distributions of biochemically diverse GIN cells, for example the CR+ versus CR− GIN cells (Caputi, Rozov, Blatow, & Monyer, 2009; Xu et al., 2006). Our colocalization study found that CR+ GIN cells are most abundant in layer II/III. Most of the CR+ GIN cells were multipolar neurons, although CR+ GIN cells could also be found in the other somatodendritic subtypes. A closer examination of the relationship between somatodendritic subtypes and CR expression might reveal a circuit-specific association of these features in the future.

The identity of GIN cells in deep layers is less investigated compared to layer II/III. In layer IV, the locally projecting quasi-fast spiking non-Martinotti cells, partially labeled in X94 mice (Ma et al., 2006), rarely exist in the GIN mice. Our reconstructions indicate that layer IV GIN cells are preferentially represented by the SST+ non-Martinotti cells with axonal projections to some extent into the supragranular layers but not into layer I (Emmenegger et al., 2018; Scala et al., 2018). In layer V, GIN cells are mainly represented by fanning-out Martinotti cells, which innervate most extensively layer II/III, and to a lesser extent layer I (Ma et al., 2006; Nigro et al., 2018).

Previous studies suggest that the origin of the axon is strongly related to somatodendritic morphology of both, pyramidal neurons and interneurons (Hamada, Goethals, de Vries, Brette, & Kole, 2016; Höfflin et al., 2017). Interneurons with more vertical dendritic distribution like

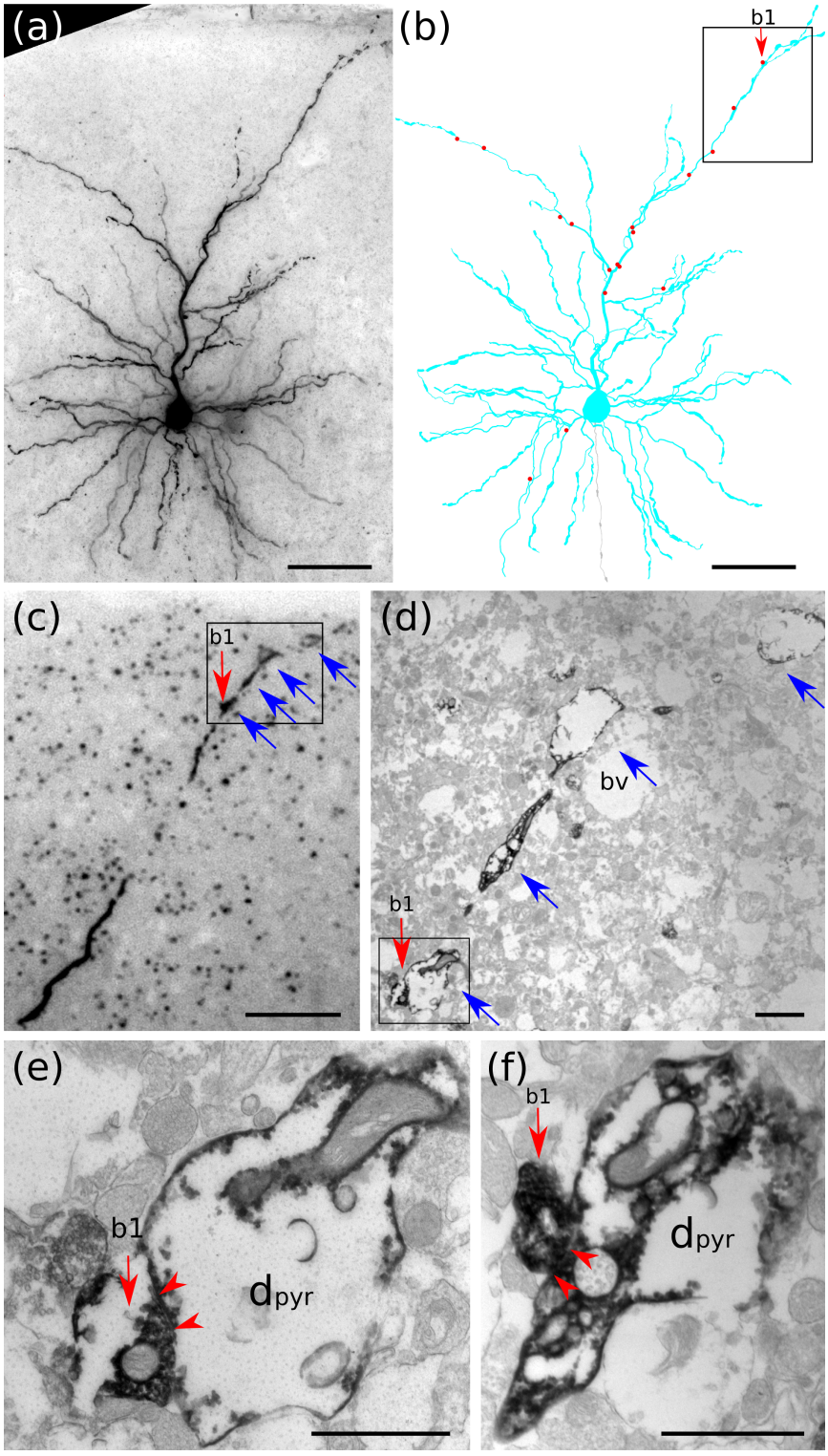


**FIGURE 9** Innervation of a biocytin-filled pyramidal neuron by GIN cell boutons. (a) A layer II/III pyramidal neuron filled with biocytin is visualized by DAB-peroxidase staining in a 300 μm-thick slice. (b) Reconstruction of the pyramidal neuron and the putative synapses formed by GIN cells (red dots). Inset of Figure 9b correlates with Figure 9c and contains one distal apical dendrite and three putative synapses. One is formed by presynaptic bouton b1 (red arrow). (c) Anti-GFP immunostaining shows numerous GIN cell boutons in the 2 μm-thick section through layer I. Inset of Figure 9c correlates to Figure 9d and contains four pieces of a tuft dendrite (blue arrows). The bouton (b1, red arrow) is likely to target (red arrows) a part of the apical dendrite in layer I. (d) The region corresponding the inset of Figure 9c was found in the electron microscope, containing the tuft dendrite (blue arrows). The putative synapse (b1, red arrow) is also found in the EM (inset of Figure 9d). bv is a blood vessel. (e,f) High-magnification EM images of two consecutive sections (with a gap) verify the synaptic ultrastructure with a synaptic cleft and a short postsynaptic density on the dendritic tuft ($d_{pyr}$) (red arrowheads). Scale bars: (a-b) 50 μm; (c) 20 μm; (d) 2 μm; (e,f) 1 μm. GIN, GFP-expressing inhibitory neurons

VIP+ cells and bitufted Martinotti cells are likely to have their axon emerging from dendrites (Höfflin et al., 2017; Prönneke et al., 2015; Wang et al., 2004). In our study, we also found a significant correlation of axon origin with somatodendritic subtypes: the majority of single tufted, bitufted, and modified cells derived their axon from dendrites, usually from first- or second-order branches of ascending dendrites. In contrast, multipolar GIN cells were more likely to have soma-originating axons. Further studies need to show how the different axon origins might correlate with detailed morphology and excitability of GIN cells (Thome et al., 2014).

## 4.2 | The ultrastructure of axons and synapses of GIN cells

A detailed analysis of the axonal morphology of various subtypes of interneurons shows that Martinotti cells have a higher number of

boutons and shorter inter-bouton intervals than nearly all the other types of interneurons (Karube, Kubota, & Kawaguchi, 2004). Reconstruction of individual Martinotti cells suggested that they usually have higher number of boutons than VIP+ interneurons (Prönneke et al., 2015; Walker et al., 2016). In our study, we found that the axons of GIN cells very often give rise to small boutons, which also form small synaptic junctions, in contrast to VIP+ neurons (Zhou et al., 2017). This seems to be a unique ultrastructural feature of all GIN cells without layer specificity. The efficacy of synaptic transmission is closely related to both, pre- and postsynaptic features, which determine presynaptic vesicle release probability and postsynaptic receptor availability/sensitivity (Holderith et al., 2012; Rollenhagen et al., 2015). The relative small synapses of GIN cells indicate that they might have a lower synaptic efficacy. However, our serial sectioning study found that single axons of GIN cells can make multiple (clustered) synapses onto the same dendritic target in layer I. Interestingly, a high percentage of clustered excitatory synapses was also shown by large volume 3D EM reconstruction in the hippocampus CA1 stratum lacunosum-moleculare, which turned out to be provided by entorhinal afferents (Bloss et al., 2018). Thus, it is hypothesized that the high number of boutons and synaptic clustering might compensate the low synaptic efficiency and enable sufficient dendritic inhibition of GIN cells in cortical layer I.

### 4.3 | Synaptic targets of GIN cells

Our quantitative EM study showed that GIN cells in mouse barrel cortex are exclusively dendrite-innervating neurons: 88% of the targets are dendritic shafts and around 12% are dendritic spines. There was no synaptic innervation of somata or any subcellular compartment of other GIN cells, thus GIN cells do not inhibit each other. In addition, GIN cells target exclusively the dendrites of excitatory neurons (91%) and rarely innervate inhibitory interneurons (9%). This result is consistent with previous ultrastructural studies of SST+ interneurons and Martinotti cells in various brain regions of different animal species (de Lima & Morrison, 1989; Katona et al., 1999; Markram et al., 2004; Melchitzky & Lewis, 2008; Wang et al., 2004). As the major output pattern of GIN cells in the mouse barrel cortex resembles that of Martinotti cells, the connectivity of layer II/III SST+ interneurons with other types of interneurons, as suggested by the findings of electrophysiological studies (Jiang et al., 2013; Jiang et al., 2015; Karnani et al., 2016; Pfeffer et al., 2013), might be largely due to other SST+ cells, which are not labeled in GIN mice.

So far, it is known that as the largest population of GIN cells, Martinotti cells, participate in different circuits and thereby regulate dendritic spike generation of neighboring pyramidal neurons at their apical dendrites by lateral or feedback inhibition (Adesnik, Bruns, Taniguchi, Huang, & Scanziani, 2012; Feldmeyer, Qi, Emmenegger, & Staiger, 2018; Hilscher, Leão, Edwards, Leão, & Kullander, 2017; Murayama et al., 2009; Silberberg & Markram, 2007). The putative synapses that mapped onto the dendritic tree of a layer II/III pyramidal neuron indicate a preferential targeting of distal parts of apical dendrites by GIN cells, including both oblique branches of apical dendrites and apical dendritic tufts. A comparable study in hippocampal CA1 region also showed that pyramidal neurons receive a higher density of synapses of SST+ interneurons at the terminal ends of their apical dendrites in stratum lacunosum-moleculare (Bloss et al., 2016). In addition, our study provides ultrastructural evidence that supports the notion of Martinotti cells being specialized in inhibiting distal dendritic shafts and spines of pyramidal cells in mouse barrel cortex.

## ACKNOWLEDGMENTS

We thank Patricia Sprysch and Sandra Heinzl for their expert technical support. We thank Dr. Möck for his suggestion on the statistical analysis related to Figure 5. The work was funded by Deutsche Forschungsgemeinschaft via the CRC 889 (Cellular mechanisms of sensory processing, subproject 7 to J.F. S.) and STA 431/14-1.

## DATA AVAILABILITY STATEMENT

The data that support the findings of this study are available on request from the corresponding author. The data are not publicly available due to privacy or ethical restrictions.

## ORCID

*Xiaojuan Zhou* https://orcid.org/0000-0003-1597-7503

## REFERENCES

Adesnik, H., Bruns, W., Taniguchi, H., Huang, Z. J., & Scanziani, M. (2012). A neural circuit for spatial summation in visual cortex. *Nature*, *490* (7419), 226–231.

Ascoli, G. A., Alonso-Nanclares, L., Anderson, S. A., Barrionuevo, G., Benavides-Piccione, R., Burkhalter, A., … Yuste, R. (2008). Petilla terminology: Nomenclature of features of GABAergic interneurons of the cerebral cortex. *Nature Review Neuroscience*, *9*(7), 557–568.

Bloss, E. B., Cembrowski, M. S., Karsh, B., Colonell, J., Fetter, R. D., & Spruston, N. (2016). Structured dendritic inhibition supports branch-selective integration in CA1 pyramidal cells. *Neuron*, *89*(5), 1016–1030.

Bloss, E. B., Cembrowski, M. S., Karsh, B., Colonell, J., Fetter, R. D., & Spruston, N. (2018). Single excitatory axons form clustered synapses onto CA1 pyramidal cell dendrites. *Nature Neuroscience*, *21*(3), 353–363.

Caputi, A., Rozov, A., Blatow, M., & Monyer, H. (2009). Two Calretinin-positive GABAergic cell types in layer 2/3 of the mouse Neocortex provide different forms of inhibition. *Cerebral Cortex*, *19*(6), 1345–1359.

Cauli, B., Zhou, X., Tricoire, L., Toussay, X., & Staiger, J. F. (2014). Revisiting enigmatic cortical calretinin-expressing interneurons. *Frontiers in Neuroanatomy*, *8*, 52.

de Lima, A. D., & Morrison, J. H. (1989). Ultrastructural analysis of somatostatin-immunoreactive neurons and synapses in the temporal and occipital cortex of the macaque monkey. *The Journal of Comparative Neurology*, *283*(2), 212–227.

DeFelipe, J., López-Cruz, P. L., Benavides-Piccione, R., Bielza, C., Larrañaga, P., Anderson, S., … Ascoli, G. A. (2013). New insights into the classification and nomenclature of cortical GABAergic interneurons. *Nature Review Neuroscience*, *14*(3), 202–216.

Domínguez, L., Morona, R., González, A., & Moreno, N. (2013). Characterization of the hypothalamus of *Xenopus laevis* during development. I. The alar regions. *The Journal of Comparative Neurology*, *521*(4), 725–759.

Emmenegger, V., Qi, G., Wang, H., & Feldmeyer, D. (2018). Morphological and functional characterization of non-fast-spiking GABAergic interneurons in layer 4 microcircuitry of rat barrel cortex. *Cerebral Cortex*, *28*(4), 1439–1457.

Fairen, A., DeFelipe, J., & Regidor, J. (1984). Nonpyramidal neurons: General account. In A. Peters & E. G. Jones (Eds.), *The cerebral cortex. Vol 1, cellular components of the cerebral cortex* (pp. 201–253). New York, NY: Plenum Press.

Feldmeyer, D., Qi, G., Emmenegger, V., & Staiger, J. F. (2018). Inhibitory interneurons and their circuit motifs in the many layers of the barrel cortex. *Neuroscience*, *368*, 132–151.

Gentet, L. J., Kremer, Y., Taniguchi, H., Huang, Z. J., Staiger, J. F., & Petersen, C. C. H. (2012). Unique functional properties of somatostatin-expressing GABAergic neurons in mouse barrel cortex. *Nature Neuroscience*, *15*(4), 607–612.

Gonchar, Y., Wang, Q., & Burkhalter, A. (2008). Multiple distinct subtypes of GABAergic neurons in mouse visual cortex identified by triple Immunostaining. *Frontiers in Neuroanatomy*, *1*, 3.

Halabisky, B., Shen, F., Huguenard, J. R., & Prince, D. A. (2006). Electrophysiological classification of somatostatin-positive interneurons in mouse sensorimotor cortex. *Journal of Neurophysiology*, *96*(2), 834–845.

Hamada, M. S., Goethals, S., de Vries, S. I., Brette, R., & Kole, M. H. P. (2016). Covariation of axon initial segment location and dendritic tree normalizes the somatic action potential. *Proceedings of the National Academy of Sciences of the United States of America*, *113*(51), 14841–14846.

He, M., Tucciarone, J., Lee, S., Nigro, M. J., Kim, Y., Levine, J. M., … Huang, Z. J. (2016). Strategies and tools for combinatorial targeting of GABAergic neurons in mouse cerebral cortex. *Neuron*, *91*(6), 1228–1243.

Hilscher, M. M., Leão, R. N., Edwards, S. J., Leão, K. E., & Kullander, K. (2017). Chrna2-Martinotti cells synchronize layer 5 type a pyramidal cells via rebound excitation. *PLoS Biology*, *15*(2), e2001392–e2001392.

Höfflin, F., Jack, A., Riedel, C., Mack-Bucher, J., Roos, J., Corcelli, C., … Engelhardt, M. (2017). Heterogeneity of the axon initial segment in interneurons and pyramidal cells of rodent visual cortex. *Frontiers in Cellular Neuroscience*, *11*, 332.

Holderith, N., Lorincz, A., Katona, G., Rózsa, B., Kulik, A., Watanabe, M., & Nusser, Z. (2012). Release probability of hippocampal glutamatergic terminals scales with the size of the active zone. *Nature Neuroscience*, *15*(7), 988–997.

Jiang, X., Shen, S., Cadwell, C. R., Berens, P., Sinz, F., Ecker, A. S., … Tolias, A. S. (2015). Principles of connectivity among morphologically defined cell types in adult neocortex. *Science*, *350*(6264), aac9462.

Jiang, X., Wang, G., Lee, A. J., Stornetta, R. L., & Zhu, J. J. (2013). The organization of two novel cortical interneuronal circuits. *Nature Neuroscience*, *16*(2), 210–218.

Karnani, M. M., Jackson, J., Ayzenshtat, I., Sichani, A. H., Manoocheri, K., Kim, S., & Yuste, R. (2016). Opening holes in the blanket of inhibition: Localized lateral disinhibition by VIP interneurons. *The Journal of Neuroscience*, *36*(12), 3471–3480.

Karube, F., Kubota, Y., & Kawaguchi, Y. (2004). Axon branching and synaptic bouton phenotypes in GABAergic nonpyramidal cell subtypes. *The Journal of Neuroscience*, *24*(12), 2853–2865.

Katona, I., Acsády, L., & Freund, T. F. (1999). Postsynaptic targets of somatostatin-immunoreactive interneurons in the rat hippocampus. *Neuroscience*, *88*(1), 37–55.

Kawaguchi, Y., & Kondo, S. (2002). Parvalbumin, somatostatin and cholecystokinin as chemical markers for specific GABAergic interneuron types in the rat frontal cortex. *Journal of Neurocytology*, *31*(3–5), 277–287.

Kawaguchi, Y., & Kubota, Y. (1996). Physiological and morphological identification of somatostatin- or vasoactive intestinal polypeptide-containing cells among GABAergic cell subtypes in rat frontal cortex. *The Journal of Neuroscience*, *16*(8), 2701–2715.

Kubota, Y., & Kawaguchi, Y. (2000). Dependence of GABAergic synaptic areas on the interneuron type and target size. *The Journal of Neuroscience.*, *20*(1), 375–386.

Lee, S., Kruglikov, I., Huang, Z. J., Fishell, G., & Rudy, B. (2013). A disinhibitory circuit mediates motor integration in the somatosensory cortex. *Nature Neuroscience*, *16*(11), 1662–1670.

Ma, Y., Hu, H., Berrebi, A. S., Mathers, P. H., & Agmon, A. (2006). Distinct subtypes of Somatostatin-containing neocortical interneurons revealed in transgenic mice. *The Journal of Neuroscience*, *26*(19), 5069–5082.

Markram, H., Toledo-Rodriguez, M., Wang, Y., Gupta, A., Silberberg, G., & Wu, C. (2004). Interneurons of the neocortical inhibitory system. *Nature Review Neuroscience*, *5*(10), 793–807.

McGarry, L. M., Packer, A. M., Fino, E., Nikolenko, V., Sippy, T., & Yuste, R. (2010). Quantitative classification of somatostatin-positive neocortical interneurons identifies three interneuron subtypes. *Frontiers in Neural Circuits*, *4*, 12.

Melchitzky, D. S., & Lewis, D. A. (2008). Dendritic-targeting GABA neurons in monkey prefrontal cortex: Comparison of somatostatin- and calretinin-immunoreactive axon terminals. *Synapse*, *62*(6), 456–465.

Muñoz, W., Tremblay, R., Levenstein, D., & Rudy, B. (2017). Layer-specific modulation of neocortical dendritic inhibition during active wakefulness. *Science*, *355*(6328), 954–959.

Murayama, M., Pérez-Garci, E., Nevian, T., Bock, T., Senn, W., & Larkum, M. E. (2009). Dendritic encoding of sensory stimuli controlled by deep cortical interneurons. *Nature*, *457*(7233), 1137–1141.

Nigro, M. J., Hashikawa-Yamasaki, Y., & Rudy, B. (2018). Diversity and connectivity of layer 5 Somatostatin-expressing interneurons in the mouse barrel cortex. *The Journal of Neuroscience*, *38*(7), 1622–1633.

Ohira, K., Takeuchi, R., Iwanaga, T., & Miyakawa, T. (2013). Chronic fluoxetine treatment reduces parvalbumin expression and perineuronal nets in gamma-aminobutyric acidergic interneurons of the frontal cortex in adult mice. *Molecular Brain*, *6*(1), 43.

Oliva, A. A., Jiang, M., Lam, T., Smith, K. L., & Swann, J. W. (2000). Novel hippocampal Interneuronal subtypes identified using transgenic mice that express green fluorescent protein in GABAergic interneurons. *The Journal of Neuroscience*, *20*(9), 3354–3368.

Peters, A., Palay, S. L., & Webster, H. D. (1991). The fine structure of the nervous system. In *Neurons and their supporting cells* (3rd ed.). USA: Oxford University Press.

Pfeffer, C. K., Xue, M., He, M., Huang, Z. J., & Scanziani, M. (2013). Inhibition of inhibition in visual cortex: The logic of connections between molecularly distinct interneurons. *Nature Neuroscience*, *16*, 1068–1076.

Pi, H.-J., Hangya, B., Kvitsiani, D., Sanders, J. I., Huang, Z. J., & Kepecs, A. (2013). Cortical interneurons that specialize in disinhibitory control. *Nature*, *503*, 521–524.

Prönneke, A., Scheuer, B., Wagener, R. J., Möck, M., Witte, M., & Staiger, J. F. (2015). Characterizing VIP neurons in the barrel cortex of VIPcre/tdTomato mice reveals layer-specific differences. *Cerebral Cortex*, *25*(12), 4854–4868.

Riedemann, T., Schmitz, C., & Sutor, B. (2016). Immunocytochemical heterogeneity of somatostatin-expressing GABAergic interneurons in layers II and III of the mouse cingulate cortex: A combined immunofluorescence/design-based stereologic study. *The Journal of Comparative Neurology*, *524*(11), 2281–2299.

Riedemann, T., Straub, T., & Sutor, B. (2018). Two types of somatostatin-expressing GABAergic interneurons in the superficial layers of the mouse cingulate cortex. *PLoS One*, *13*(7), e0200567.

Rollenhagen, A., Klook, K., Sätzler, K., Qi, G., Anstötz, M., Feldmeyer, D., & Lübke, J. H. R. (2015). Structural determinants underlying the high efficacy of synaptic transmission and plasticity at synaptic boutons in layer 4 of the adult rat "barrel cortex". *Brain Structure and Function*, *220*(6), 3185–3209.

Rudy, B., Fishell, G., Lee, S., & Hjerling-Leffler, J. (2011). Three groups of interneurons account for nearly 100% of neocortical GABAergic neurons. *Developmental Neurobiology*, *71*(1), 45–61.

Scala, F., Kobak, D., Shan, S., Bemaerts, Y., Latumus, S., Cadwell, C. R., … Tolias, A. S. (2018). Neocortical layer 4 in adult mouse differs in major cell types and circuit organization between primary sensory areas. Retrieved from https://www.biorxiv.org/content/10.1101/507293v2.

Silberberg, G., & Markram, H. (2007). Disynaptic inhibition between neocortical pyramidal cells mediated by Martinotti cells. *Neuron*, *53*(5), 735–746.

Somogyi, P., Hodgson, A. J., Chubb, I. W., Penke, B., & Erdei, A. (1985). Antisera to gamma-aminobutyric acid. II. Immunocytochemical application to the central nervous system. *The Journal of Histochemistry and Cytochemistry*, *33*(3), 240–248.

Staiger, J. F., Flagmeyer, I., Schubert, D., Zilles, K., Kötter, R., & Luhmann, H. J. (2004). Functional diversity of layer IV spiny neurons in rat somatosensory cortex: Quantitative morphology of Electrophysiologically characterized and Biocytin Labeled cells. *Cerebral Cortex*, *14*(6), 690–701.

Taniguchi, H., He, M., Wu, P., Kim, S., Paik, R., Sugino, K., … Huang, Z. J. (2011). A resource of Cre driver lines for genetic targeting of GABAergic neurons in cerebral cortex. *Neuron*, *71*, 995–1013.

Tasic, B., Yao, Z., Graybuck, L. T., Smith, K. A., Nguyen, T. N., Bertagnolli, D., … Zeng, H. (2018). Shared and distinct transcriptomic cell types across neocortical areas. *Nature*, *563*(7729), 72–78.

Thome, C., Kelly, T., Yanez, A., Schultz, C., Engelhardt, M., Cambridge, S. B., … Egorov, A. V. (2014). Axon-carrying dendrites convey privileged synaptic input in hippocampal neurons. *Neuron*, *83*(6), 1418–1430.

Tremblay, R., Lee, S., & Rudy, B. (2016). GABAergic interneurons in the Neocortex: From cellular properties to circuits. *Neuron*, *91*(2), 260–292.

Urban-Ciecko, J., & Barth, A. L. (2016). Somatostatin-expressing neurons in cortical networks. *Nature Review Neuroscience*, *17*(7), 401–409.

Walker, F., Möck, M., Feyerabend, M., Guy, J., Wagener, R. J., Schubert, D., … Witte, M. (2016). Parvalbumin- and vasoactive intestinal polypeptide-expressing neocortical interneurons impose differential inhibition on Martinotti cells. *Nature Communications*, *7*, 13664.

Wang, Y., Toledo-Rodriguez, M., Gupta, A., Wu, C., Silberberg, G., Luo, J., & Markram, H. (2004). Anatomical, physiological and molecular properties of Martinotti cells in the somatosensory cortex of the juvenile rat. *The Journal of Physiology*, *561*(Pt 1), 65–90.

Xu, H., Jeong, H. Y., Tremblay, R., & Rudy, B. (2013). Neocortical somatostatin-expressing GABAergic interneurons disinhibit the thalamorecipient layer 4. *Neuron*, *77*(1), 155–167.

Xu, X., Roby, K. D., & Callaway, E. M. (2006). Mouse cortical inhibitory neuron type that coexpresses somatostatin and calretinin. *The Journal of Comparative Neurology*, *499*(1), 144–160.

Zhou, X., Rickmann, M., Hafner, G., & Staiger, J. F. (2017). Subcellular targeting of VIP boutons in mouse barrel cortex is layer-dependent and not restricted to interneurons. *Cerebral Cortex*, *27*(11), 5353–5368.

**How to cite this article:** Zhou X, Mansori I, Fischer T, Witte M, Staiger JF. Characterizing the morphology of somatostatin-expressing interneurons and their synaptic innervation pattern in the barrel cortex of the GFP-expressing inhibitory neurons mouse. *J Comp Neurol*. 2020;528:244–260. https://doi.org/10.1002/cne.24756